

Catalog of magnetic white dwarfs with hydrogen dominated atmospheres

L. L. AMORIM,¹ S. O. KEPLER,¹ BAYBARS KÜLEBI,² S. JORDAN,³ AND A. D. ROMERO¹

¹*Instituto de Física, Universidade Federal do Rio Grande do Sul, 91501-900 Porto-Alegre, RS, Brazil*

²*Institut de Ciències de l'Espai, Universitat Autònoma de Barcelona and Institute for Space Studies of Catalonia, Gran Capita 2-4, Edif. Nexus 104, E-08034 Barcelona, Spain*

³*Astronomisches Rechen-Institut, Zentrum für Astronomie der Universität Heidelberg, Mönchhofstr. 12-14, D-69120 Heidelberg, Germany*

ABSTRACT

White dwarfs are excellent research laboratories as they reach temperatures, pressures, and magnetic fields that are unattainable on Earth. To better understand how these three physical parameters interact with each other and with other stellar features, we determined the magnetic field strength for a total of 804 hydrogen-rich white dwarfs of which 287 are not in the literature. We fitted the spectra observed with the Sloan Digital Sky Survey using atmospheric models that consider the Zeeman effect due to the magnetic field at each point in the stellar disk. Comparing magnetic and non-magnetic WDs, the literature already shows that the magnetic ones have on average higher mass than the non-magnetic. In addition to that, magnetic fields are more common in cooler WDs than in hotter WDs. In consonance, we found that those with higher magnetic field strengths tend to have higher masses, and lower temperatures, for which models indicate the crystallization process has already started. This reinforces the hypothesis that the field is being generated and/or amplified in the cooling process of the white dwarf. Our sample constitutes the largest number of white dwarfs with determined magnetic fields to date.

Keywords: White dwarf stars (1799) — DA stars (348) — Stellar magnetic fields (1610)

1. INTRODUCTION

Strong magnetic fields are common in Hydrogen-rich white dwarfs stars (DAs). Kepler et al. (2013) showed that at least 4% of all DAs observed with *Sloan Digital Sky Survey* (SDSS) until Data Release 7 have magnetic fields greater than 1 MG. The authors visually inspected all DA spectra and found 521 stars with Zeeman Splittings. A more robust method to determine the field was presented by Külebi et al. (2009), who used least squares minimization to find the best model of magnetic field geometry to fit the observed spectra. They applied this technique to 141 magnetic white dwarfs rich in hydrogen (DAH). A revisit to the previous measurements is insightful, since the largest work with DAHs considered only the splitting in H-alpha and H-beta and used only a visual field determination method. We want complete and homogeneous results to try to understand general properties of these stars to add information to the question of the origin of the magnetic fields. In this work, we use the fitting method to measure the magnetic field of all 804 DAHs found in the SDSS sample until Data Release 16 (DR16). From this, 287 are newly reported DAHs.

The fraction of detected magnetic white dwarfs depends on the observed sample, the detection method, and spectral types. Bagnulo & Landstreet (2021) found 23.4 ± 4.8 % of DAHs in the DA volume-limited sample for 20 pc using spectropolarimetry, while Kepler et al. (2013) encountered 4% of DAHs in the DAs of a SDSS magnitude limited sample with spectroscopy only. Kawka (2020) presents a table of differences in the fraction of magnetic white dwarfs through various spectral types. The fraction of detected magnetic white dwarfs may differ from the real fraction of magnetic white dwarfs due to limitations on the domain of magnetic field strength studied, the quality of the data, or the significance of the measurable physical effect.

The origin of magnetic fields in white dwarfs is still an open question after more than fifty years of the first discovery by Kemp et al. (1970). A systematic study is crucial for the construction of a significant statistical sample, which may help us shed some light on their origin. The magnetic field could be formed in three different stages of the white dwarf evolution: before the white dwarf stage, during its formation, or during the cooling process.

The main hypothesis of the first group corresponds to the fossil fields from Ap/Bp stars (chemically peculiar and with magnetic fields stronger than classical A- or B-type stars). The original gas from which stars are formed are probably magnetized, since the net magnetic field of the galaxy is not zero. In the main sequence, these fields are usually small, of the order of a few kG as first shown by Babcock (1947) and later examples in Babcock (1958). The magnetic field can be boosted through conservation of the magnetic flux up to 100 MG when the star gets stripped of its outer layers and its core gets exposed and starts to contract during the white dwarf cooling sequence.

This possible origin of the magnetic field is very attractive because the Ohmic decay in degenerate matter suggests that these fields should last billions of years. However, Wickramasinghe & Ferrario (2005) concluded that the amount of magnetic Ap/Bp stars that have been detected cannot account for the fraction of magnetic white dwarfs (MWD) measured, so other mechanisms must also occur.

For the magnetic field to arise during the formation of the white dwarf, the system may not be single. It can be due to the merger of two degenerate cores, or it can be formed during the interaction of the two components of the binary (common envelope) as presented by Tout et al. (e.g. 2008). However, this channel of magnetism formation would lead to a much higher magnetic incidence among white dwarfs in close binaries than is currently observed (e.g Belloni & Schreiber 2020).

Liebert (1988) was the first to suggest that magnetic WDs have generally a higher mass than non-magnetic WDs. This was consistently found in several subsequent works, such as Kepler et al. (2013) and McCleery et al. (2020). Bagnulo & Landstreet (2021) argued that the fact that the magnetic have, in average, a higher mass than the non-magnetic is true only for young WDs. The possible origins mentioned so far are in agreement with the higher mass that MWDs have when compared to the whole sample.

Nevertheless, there is evidence of yet another way of forming magnetic fields in white dwarfs. It was early supposed that magnetic fields are more common and stronger in cooler white dwarfs because it was first detected in this group (Greenstein et al. (1971)). Eventually, hot magnetic white dwarfs were also detected, and the early result was indeed corroborated (Liebert & Sion (1979)). The sample was still subjected to strong selection effects and the results were questioned. Valyavin & Fabrika (1999) studied the evolution of magnetic white dwarfs in an even larger sample and concluded that as the star cools, the frequency of magnetic white dwarfs increases, as does the strength of the magnetic fields detected. This was endorsed by further studies such as Kepler et al. (2013) and Bagnulo & Landstreet (2021). This means that the white dwarf must be producing, exposing or enhancing the surface magnetic field.

When a DA white dwarf cools below 14000 K, it develops a surface convective layer in which the dynamo process can occur, giving a boost to the surface field. However, as the temperature continues to drop, the kinetic energy of the envelope becomes larger, and eventually the convective cells hinder the magnetic field line movement. This is coherent with the further drop of magnetic field strength at even lower temperatures.

We could also mention other possibilities that could account for the magnetic field in white dwarfs, like the crystallization of its core (Isern et al. 2017; Ginzburg et al. 2022) and the interaction with orbiting planets (Schreiber et al. 2021). The later effect will not be further studied in this work, as we have yet no evidence that it is statistically significant to the complete sample.

2. DETECTION OF MAGNETIC FIELDS IN SDSS DR16 WHITE DWARFS

To build our sample, we visually investigated all DA spectra from Sloan Digital Sky Survey (SDSS) DR7 to DR16 searching for Zeeman Splittings and concatenated the selected ones with the previously known until Data Release 7, resulting in a total of 804 magnetic white dwarfs with SDSS spectra. We used the code (YAWP) presented by Külebi et al. (2009) to determine the strength of the magnetic fields across the surface of the star which better matches the observed spectrum, assuming an off-center dipole inclined in relation to our line of sight.

Our results are presented in Table 2. To exemplify, Figure 1 shows three white dwarfs with magnetic field strengths of different orders of magnitude. The values presented are compatible with previous determinations within the uncertainties. We chose to use a fixed temperature extracted from the photometry of SDSS, while Külebi et al. (2009) allowed it to be a free parameter in the fit. Kepler et al. (2013) only computed a visual estimate of the magnetic field considering only the spectral line positions. The comparison of these different methods is presented in Figure 2.

The inclination and offset of the dipole are correlated quantities in our models. Different combinations between them can result in distributions of the magnetic field over the stellar surface for which the effect measured in one spectrum is the same. With that in mind, we interpret them as a measurement of the complexity of the field over the stellar surface and not necessarily a reflection of unique parameters.

Table 1. The table presents the identifiers of the DAHs in the SDSS and their masses and effective temperatures calculated with Gaia astrometry presented in [Gentile Fusillo et al. \(2021\)](#) when available. T_{SDSS} is the temperature we used for the magnetic field model, computed using non-magnetic atmospheric models and SDSS colors g, r, and i. The following columns present the parameters of the magnetic field resulting from the best YAWP model for each star. In order, there is the the dipole magnetic field strength of the offset dipole, the uncertainty computed through least squares, the z-offset from the center, and the inclination of the dipole to the line of sight. We call the attention that these last two quantities should be interpreted as a reference for the magnetic field structure (how different from a regular dipole) because there are degeneracies, especially due to changes in the field structure as the star rotates. The full table is available as online supporting information.

SDSS	Plate-MJD-Fiber	M (M_{\odot})	T_{eff} (K)	T_{SDSS} (K)	B (MG)	$\sigma(B)$ (MG)	z_{offset} (R_{*})	incl($^{\circ}$)
J113212.99-003036.8	0282-51658-0278	—	—	20000	3.19	0.46	0.04	21.79
J114720.40-002405.7	0283-51584-0120	0.68	15919	17000	2.00	—	—	33.47
J121105.25-004628.5	0287-52023-0253	1.34	27473	19500	2.56	0.01	-0.32	66.65
J121635.36-002656.3	0288-52000-0276	—	—	15000	64.24	0.11	-0.18	59.27
J130807.48-010117.0	0294-51986-0089	0.47	11757	18500	2.20	0.00	-0.21	72.94
J144114.21+003702.3	0307-51663-0595	0.87	25472	21000	4.39	0.49	0.49	20.70
J112852.88-010540.7	0326-52375-0565	—	—	18000	2.81	0.36	0.36	0.08
J113431.97-031529.0	0327-52294-0131	1.24	14539	15500	3.00	0.01	0.34	16.44
J155238.20+003910.4	0342-51691-0639	1.26	14285	12500	2.16	0.08	0.12	41.32
J171556.26+600643.7	0354-51792-0318	0.55	13567	9500	2.07	0.01	0.17	27.63
J172932.48+563204.1	0358-51818-0239	—	—	10000	6.00	0.04	0.49	0.46
J172329.14+540755.7	0359-51821-0415	1.09	10175	10000	36.82	6.75	-0.05	53.78
J173915.64+545059.1	0360-51816-0547	0.30	9376	16000	2.69	0.02	0.37	31.91
J173235.19+590533.3	0366-52017-0591	0.57	11028	11500	2.56	0.04	-0.36	78.63
J171441.07+552711.3	0367-51997-0318	—	—	30000	6.45	1.80	0.47	3.84
J172045.35+561214.8	0367-51997-0461	—	—	15000	24.67	0.01	-0.30	78.71
J220435.05+001242.9	0372-52173-0626	1.11	10502	10500	2.15	0.00	0.13	12.83
J220823.65-011534.1	0373-51788-0086	0.39	19044	9500	3.04	0.11	-0.50	35.80
J220514.08-005841.6	0373-51788-0243	0.75	18464	14500	3.01	0.02	0.42	74.80
J221828.58-000012.1	0374-51791-0583	1.06	12806	12239	220.78	6.35	-0.04	24.85
J231432.89-011320.3	0382-51816-0289	—	—	18500	4.50	0.00	0.45	4.02
J232248.21+003901.0	0383-51818-0421	1.17	18130	11500	21.20	0.49	-0.38	33.30
J022335.15+004954.8	0406-51900-0490	0.54	6728	9500	2.16	0.02	-0.15	65.68
J022523.67+002743.0	0406-51900-0543	—	—	15500	2.02	0.00	0.16	0.16
J022623.80-002313.1	0406-52238-0071	—	—	16500	1.30	0.12	0.00	33.47
J025837.19+000019.2	0410-51877-0065	0.75	10561	10000	2.33	0.01	0.16	2.51
J032137.43+010437.3	0413-51821-0578	0.89	21140	18000	2.86	0.00	0.05	16.68
J031323.65-001659.9	0413-51929-0313	—	—	30000	7.30	0.00	0.42	0.00
J033145.69+004516.9	0415-51879-0378	1.05	19230	12000	13.05	2.37	-0.42	48.36
J033320.37+000720.6	0415-51879-0485	0.79	7498	9500	771.71	214.35	0.18	0.10
J034511.10+003444.2	0416-51811-0590	0.57	7431	8000	2.50	0.27	-0.36	12.91
J003111.75+134919.5	0417-51821-0084	—	—	21000	2.24	0.00	0.15	0.72
J003232.07+153126.6	0418-51817-0346	0.35	9917	17000	2.00	0.78	0.10	15.36
J004513.88+142248.1	0419-51879-0147	0.81	7629	8000	3.61	0.04	-0.29	18.68
J013533.20+132249.8	0426-51882-0291	—	—	21000	5.10	0.01	0.00	33.47
J013920.54+152218.7	0426-51882-0524	0.46	10530	18000	2.30	0.00	0.19	0.56
J021230.00+122557.2	0428-51883-0046	—	—	15500	2.07	0.11	0.14	0.80
J075959.57+433521.1	0437-51869-0369	—	—	9000	91.55	57.78	-0.38	29.35
J081136.33+461156.4	0439-51877-0523	—	—	40000	4.95	2.77	0.49	3.90
J085159.32+532540.3	0449-51900-0311	0.87	11106	11500	63.76	28.16	-0.17	13.81

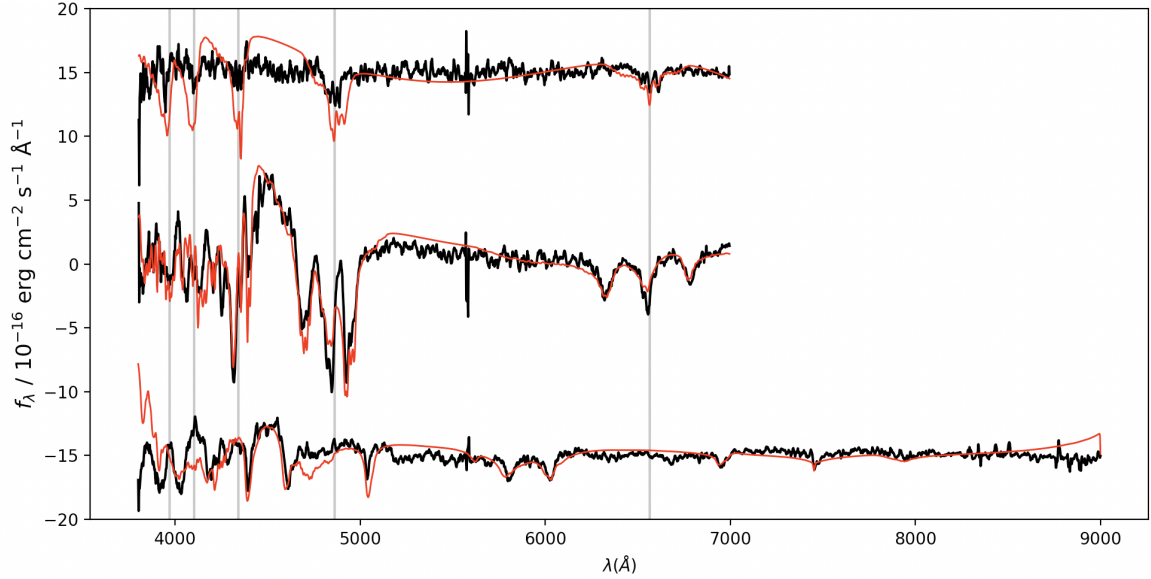


Figure 1. SDSS spectrum of three of the stars we computed the magnetic field. The model with the best least-squares fit to the observed data is shown in red. From top to bottom we have (a) SDSS J101529.62+090703.7, Plate-MJD-Fiber = 1237-52762-0533, $B = 2.51$ MG, $S/N = 12$ and $T_{\text{eff}} = 8000$ K; (b) SDSS J215148.31+125525.2, Plate-MJD-Fiber = 0733-52207-0522, $B = 20.71$ MG, $S/N = 20$ and $T_{\text{eff}} = 10000$ K; (c) SDSS J134845.98+110008.8, Plate-MJD-Fiber = 5445-55987-0530, $B = 202.58$ MG, $S/N = 11$ and $T_{\text{eff}} = 16500$ K. We corrected with a third degree polynomial function the inclination of the spectra and attributed an arbitrary shift in flux for a better visualization. The gray vertical lines represent the wavelength of the Balmer lines in the regime of no magnetic field.

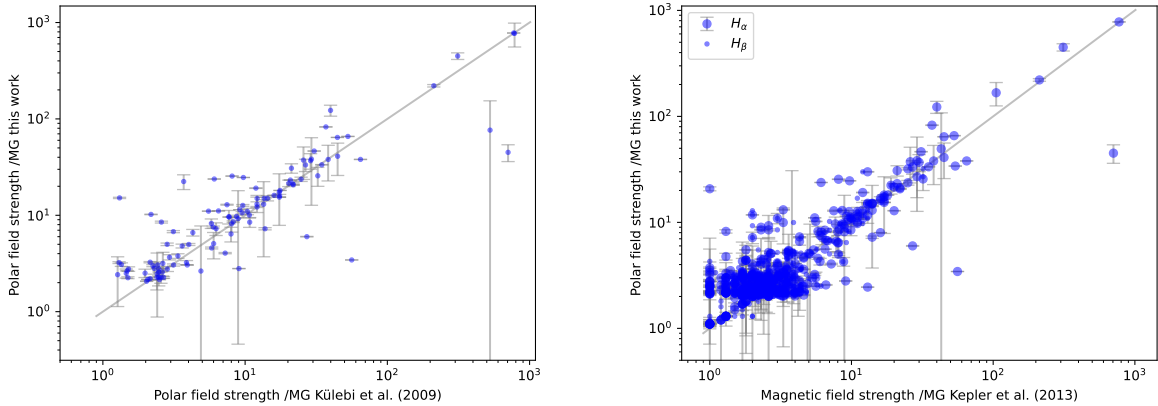


Figure 2. In the left panel, we present the comparison of dipole magnetic field strength of the offset dipole presented in this work and the values presented by Külebi et al. (2009). In the right panel, we present the comparison of dipole magnetic field strength of the offset dipole presented in this work and visually estimated values from Kepler et al. (2013); the different size dots represent the two independent lines they used to estimate the magnetic field.

The magnetic field affects the line profiles, and we cannot use them to estimate surface gravity directly. Thereby, the effect of the magnetic field in the radiation transfer in model atmospheres used in the code were calculated with $\log g = 8$ for all the stars as an approximation. This value was originally chosen to consider that it is the mean value for white dwarfs. We acknowledge that it is not the best value to represent magnetic white dwarfs once they were found to be more massive than non-magnetic ones. Fortunately, this doesn't affect the position of the lines that are closely related to the magnetic field strength, only their strength.

The code also presents the possibility of searching for the temperature spectroscopically, together with the magnetic field parameters. But, due to the uncertainties in the spectra and the surface gravity versus effective temperature

correlation, we opted to use a previously estimated temperature acquired by comparing the observed fluxes with hydrogen-rich atmospheric models. These models lead to a table of colors in the bands u, g, r, i, and z used by SDSS for each temperature. One can compare these values, especially their differences (color index), to the values from the observed spectra, thus obtaining an estimated temperature. We chose not to use the z-band since it is observed a lot of noise in the corresponding wavelengths. The u-band was also discarded since it is expected to be the most affected by the magnetic splitting of the lines.

We only fitted temperatures between 8000 K and 40000 K when varying the magnetic field due to convergence problems. For only one star out of 4 which we should have used 50000 K we were able to find a model with this temperature. No model was found with appropriate temperatures for the 13 stars cooler 8000 K. This limits our capacity to model the magnetic field of these stars, as the models present deeper lines than those observed in the SDSS spectra, partially due to the $\log g=8.0$ approximation. The depth of the absorption lines does not have a large impact on the determination of the magnetic field amplitudes, which are predominantly determined by the wavelength displacement and presence of splittings. This effect can be seen in the upper part of Figure 1, in which a WD with a temperature below 8000 K is presented. The best model, in red, clearly has lines deeper than the observed spectra but well represents the splitting on the $H_\alpha = 6565 \text{ \AA}$ and $H_\beta = 4861 \text{ \AA}$ lines.

For better visualization, we present the observed spectra with a running mean of five points because the measured spectra are usually noisy. We emphasize that this step was taken after we ran YAWP and its only purpose is to guide us in the analysis of the results. The noise in the observed spectra is wavelength-dependent and is significantly higher above 7000 \AA . It is noticeable that the hydrogen absorption lines do not reach these long wavelengths for field regimes below 25 MG ($\log B \approx 1.4$), as can be seen in Figure 3 from Schimeczek & Wunner (2014). Therefore we do not consider higher wavelengths in the spectra of DAHs with lower fields to minimize the noise effect, which can be seen in the first two spectra of Figure 1.

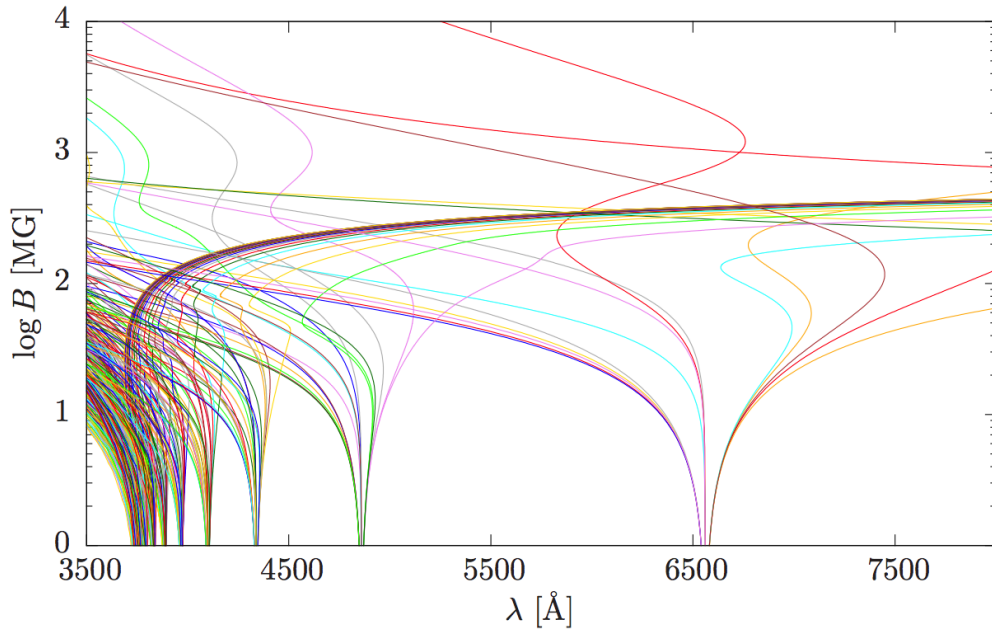


Figure 3. Magnetic field strength as a function of the wavelength of the first 325 transitions in the Balmer series, which emerge from the field-free Balmer transitions up to principal quantum numbers $n = 10$. Colors were arbitrarily assigned to facilitate visualization. Figure from Schimeczek & Wunner (2014)

For some stars, YAWP did not converge to a solution, and we resorted to a simpler visual analysis to estimate the magnetic field, used it as a fixed input to the code, and fitted only the inclination and the offset. An illustrative example of the visual inspection can be seen in Figure 4.

After we determined a magnetic field strength visually, we computed the best model with the magnetic field fixed and varying only the inclination and offset. One example is portrayed in Figure 5. In this specific case, YAWP did

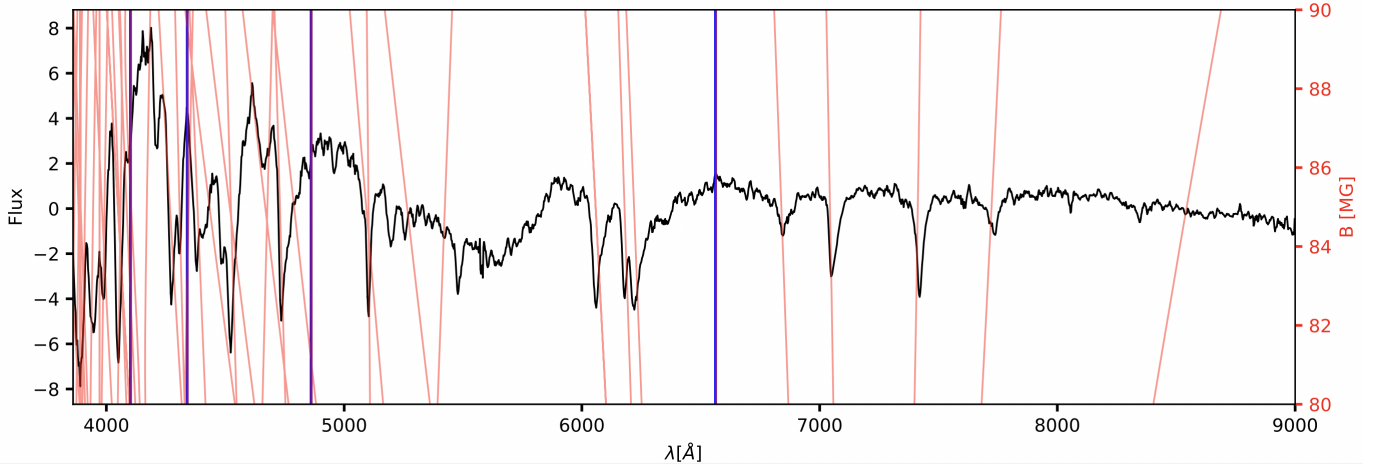


Figure 4. Spectra of DAH after applying the smooth function and normalizing by a third-degree polynomial function for better display. The star SDSSJ085649.67+253441.0 in the plot has Plate-MJD-Fiber = 5179-55957-0778, $B = 85$ MG, $S/N = 14$, and $T_{\text{eff}} = 11\,500$ K. The flux is $f_{\lambda} / 10^{-16} \text{ erg cm}^{-2} \text{ s}^{-1} \text{ \AA}^{-1}$. The red lines represent the magnetic field strength as a function of the wavelength, as computed by Schimeczek & Wunner (2014). The blue vertical lines represent the position of absorption lines for hydrogen when no magnetic field is applied.

not converge to the best solution on its own, most probably due to the possible contamination of a very close star in the field.

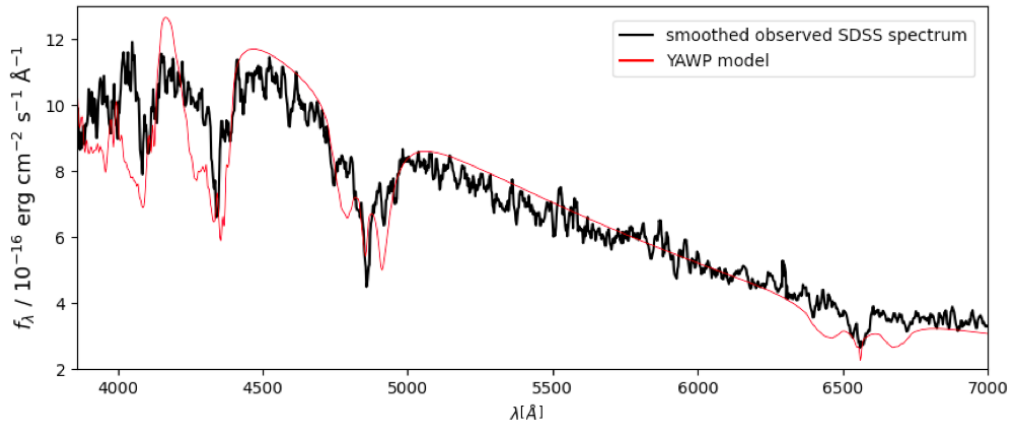


Figure 5. SDSS spectrum of the star with SDSS J004248.20+001955.2 is presented in black. The model with the best least-squares fit to the observed data with Plate-MJD-Fiber = 0690-52261-0594, $B = 8.5$ MG, $S/N = 7.5$ and $T_{\text{eff}} = 14\,000$ K is shown in red. Even though we plot the whole spectrum, the continuum is not used in the fit.

The visual estimation was also used for four stars with magnetic fields below 1 MG and S/N above 10. The magnetic field values were not used as input for YAWP since it is out of the range comprised in the models. An example can be seen in Figure 6.

The only geometry of magnetic fields considered for our determinations was the non-centered dipole, which was a good approximation for these objects. Therefore, the difference in magnetic field strength between stellar surface regions is substantial, up to orders of magnitude, and is larger with increasing polar field strength. Some exceptions exist, such as if the inclination is close to 90 deg, and we look straight into a pole of a little off-centered dipole. This effect can be seen in Figure 7. The model that best reproduces the observed data has a mean modulus of magnetic field strength over the stellar surface of $B = 61$ MG (red line in the outside panel). However, this is incompatible with simply summing the respective spectra of each area element and evaluating the result. Since each magnetic field

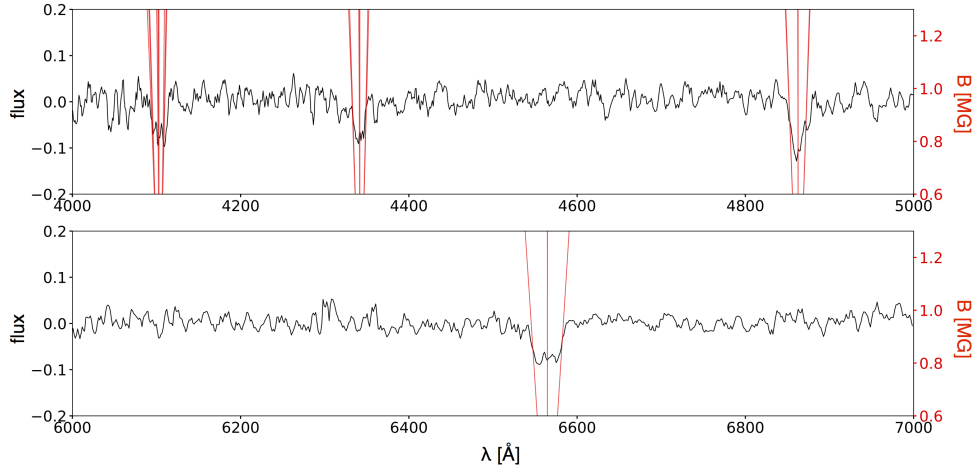


Figure 6. Spectra of the star with SDSS J090139.03+064022.4, Plate-MJD-Fiber = 4868-55895-0730, $B = 0.8$ MG, $S/N = 12$, and $T_{\text{eff}} = 8000$ K after applying the smooth function and normalizing by a third-degree polynomial function for better display. The flux is $f_{\lambda} / 10^{-16} \text{ erg cm}^{-2} \text{ s}^{-1} \text{ \AA}^{-1}$. The red lines represent the magnetic field strength as a function of the wavelength, as computed by Schimeczek & Wunner (2014).

intensity affects the line profiles in a specific way, the summed spectra will look more like the mode than the mean, in this case.

It can be seen in the inside panel of Figure 6 that about half of the stellar surface presents field intensities varying from 40 to 120 MG, while the other half presents field intensities around 30 MG. In addition, lower fields are easier to identify visually due to the lower complexity of the line profiles, as seen in Figure 3. As a consequence, if we did the visual inspection of the total spectra coming from the whole visible disk, we would find a value closer to 30 MG.

In addition to the intrinsic variation, we estimate that our precision cannot be better than 1 MG due to spectral resolution and signal-to-noise ratios. Beyond these limitations, from the χ^2 , the mean magnetic field uncertainties are approximately 12% of the computed value.

3. DISCUSSION

Liebert et al. (2003) propose that magnitude-limited samples, as the one studied in this work, have a bias against higher mass white dwarfs since for a given temperature, they have a smaller radius and consequently smaller luminosity. This would lead them to be detected less frequently. However, they did not take into consideration that more massive white dwarfs take longer to cool down because they have a smaller radius. It is not straightforward which of these effects predominates at a given time. Bagnulo & Landstreet (2021) showed that magnitude-limited samples have a complex bias against or in favor of higher masses depending on the stellar age. One can conclude that there is a bias in favor of younger stars independently of their mass. They also found that the frequency of magnetic white dwarfs is substantially depressed for stars younger than 0.5 Gyr and that this difference probably reflects the action of the mechanisms that produce magnetic fields in white dwarfs.

Even though it favors younger stars, magnitude-limited surveys, especially with low-resolution spectroscopy, are the ones that can go deeper in magnitude and examine a larger sample of stars. With this perspective, we will discuss the distribution of magnetic field strength, the relation between magnetic field and mass, effective temperature and period, and some specific cases that stand out in our sample.

3.1. Distribution of magnetic field strength

The fraction of magnetic white dwarfs rich in hydrogen found in this work was 2.7%, far below the previous values presented in the literature. We call attention to the strong bias present in our sample due to the chosen survey. The selection of which stars were observed by SDSS changed over time, resulting in a smaller number of magnetic white dwarfs in the latest data releases because white dwarfs were not specifically targeted.

We also note that the visual identification of Zeeman splittings is much more efficient for magnetic fields below 60 MG when the effect is well-behaved, as can be noticed in Figure 3. The SDSS spectral resolution around 2 \AA also hinders the detection of fields below 1 MG, even for $S/N \geq 10$. With these reservations, we present the distribution of

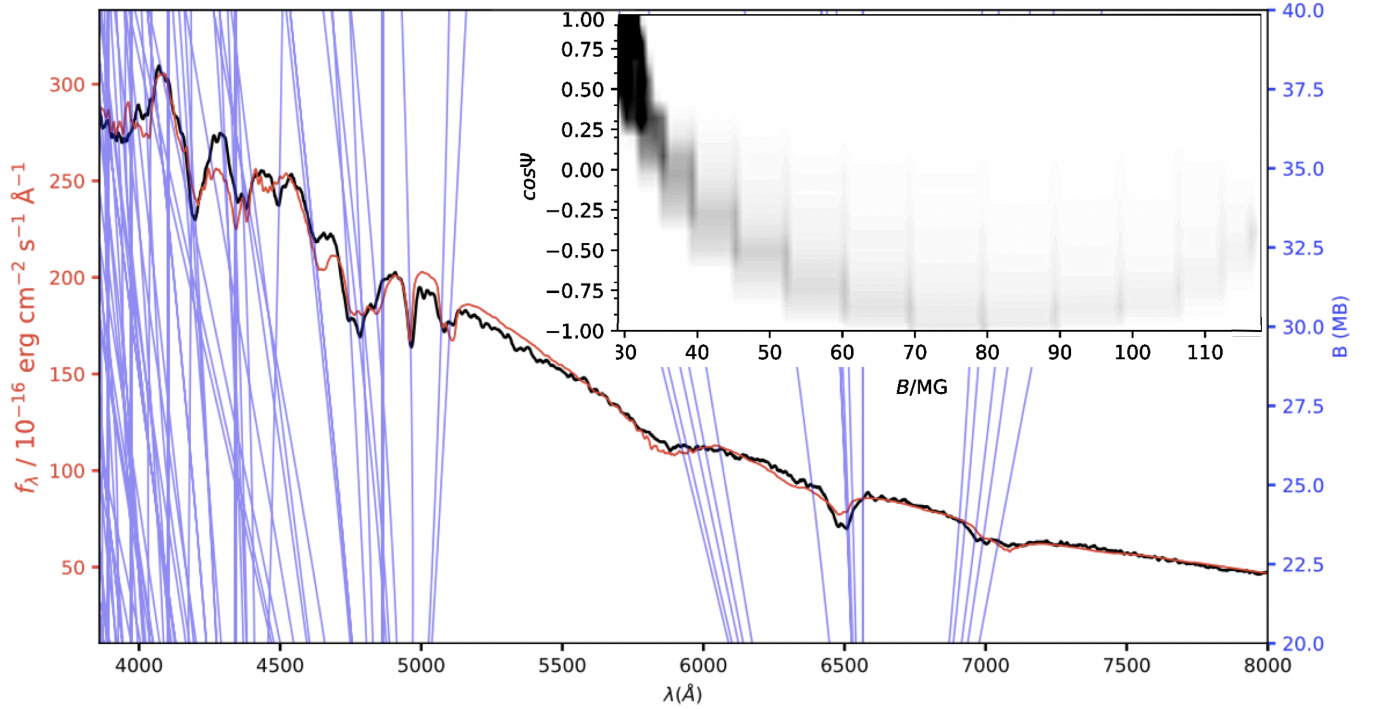


Figure 7. Outer panel showing the SDSS spectrum of the star with SDSSJ102054.10+362647.0, Plate-MJD-Fiber = 4568-55600-0952, $B = 61.2$ MG, $S/N \simeq 63$ and $T_{\text{eff}} = 13500$ K is presented in black. The model with the best least-squares fit to the observed data is shown in red. The blue lines represent the magnetic field strength as a function of the wavelength, as computed by Schimeczek & Wunner (2014). The inner panel shows the distribution of magnetic field over the stellar surface due to the inclination of 29.35° and z_{offset} of $-0.38 R_\star$ delineated by the best model.

the magnetic field strength of our sample in Figure 8. A higher appearance of magnetic fields strength below 3 MG is noticeable. It is not in all cases evident that the stars are magnetic due to the limited SDSS S/N.

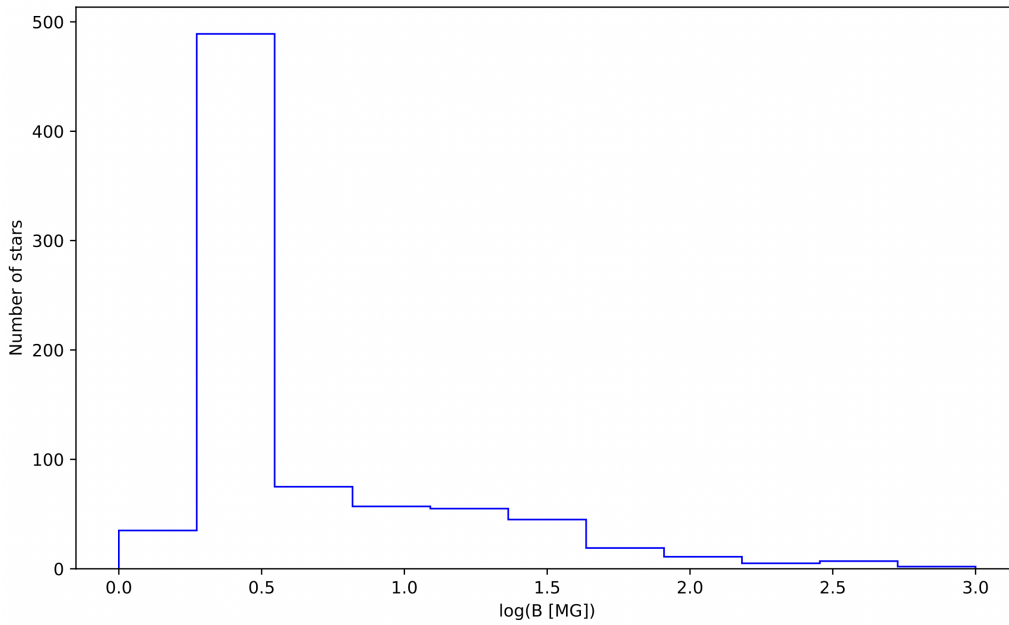


Figure 8. Magnetic field strength histogram for all magnetic white dwarf in our sample.

3.2. Relation between mass and magnetic field

To examine the possible relation between magnetic field and mass, we made the Figure 9 to study the fraction of stars with magnetic fields, and Figure 10 to study the connection between the strength of the magnetic field and the star's mass.

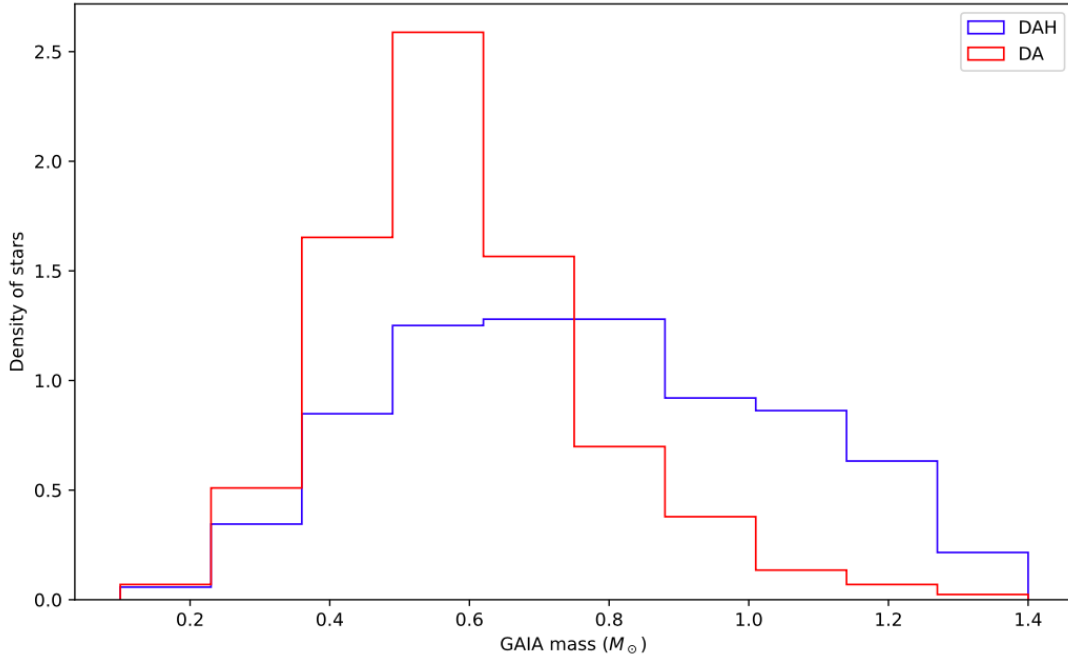


Figure 9. Histogram of mass calculated with Gaia data for all DAs in red and only the magnetic ones in blue.

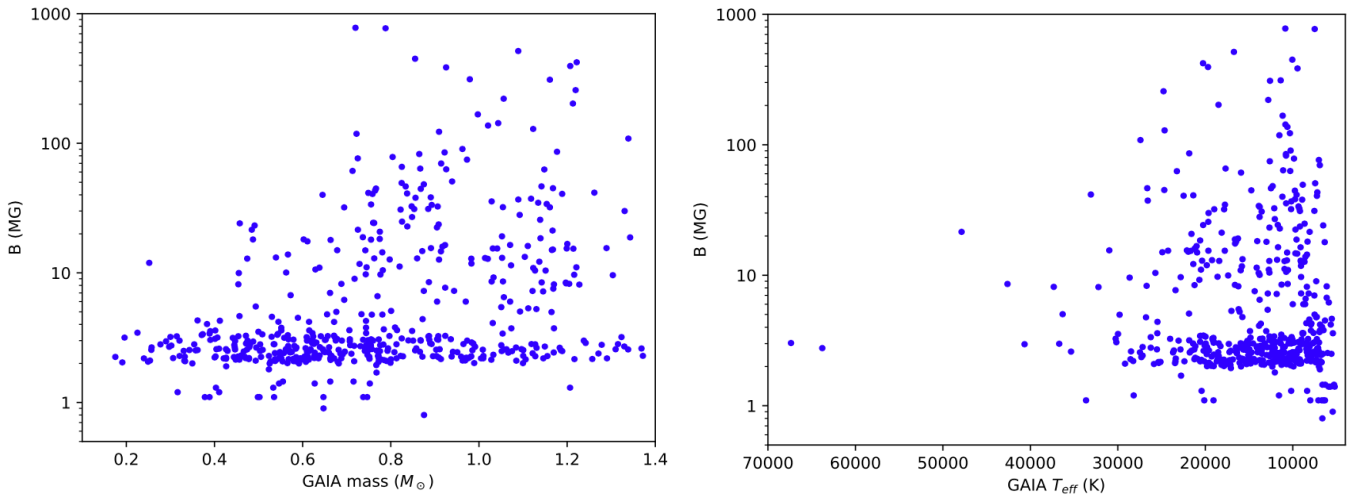


Figure 10. Magnetic field versus mass calculated with Gaia data, showing a clear absence of highly magnetic white dwarfs with lower masses on the left. Magnetic field versus effective temperature calculated with Gaia data, showing a clear increase of highly magnetic white dwarfs with lower temperatures on the right.

It appears that the distribution of mass of DAHs can be approximated by a Gaussian centered in $0.78 M_{\odot}$ with no further remarkable features. The left panel in Figure 10 shows an evident lack of low mass DAHs with strong fields.

3.3. Relation between effective temperature and magnetic field

In the search for a hint of the magnetic field origin, we investigate its relation to the effective temperature of the inspected stars. The right panel in Figure 10 shows that the magnetic field strength increases as the effective temperature decreases.

Not only do we find white dwarfs with stronger magnetic fields, but also we detect more magnetic white dwarfs at lower temperatures. The second effect is naturally expected because it is easier to detect white dwarfs at lower temperatures since they spend more time cooling down. To consider this effect and check if there are really more magnetic white dwarfs at lower temperatures, we study the fraction of DAHs compared to the whole sample of white dwarfs rich in hydrogen. This is illustrated by Figure 11, and it is noticeable that the fraction of magnetic stars is indeed increasing as the temperature decreases.

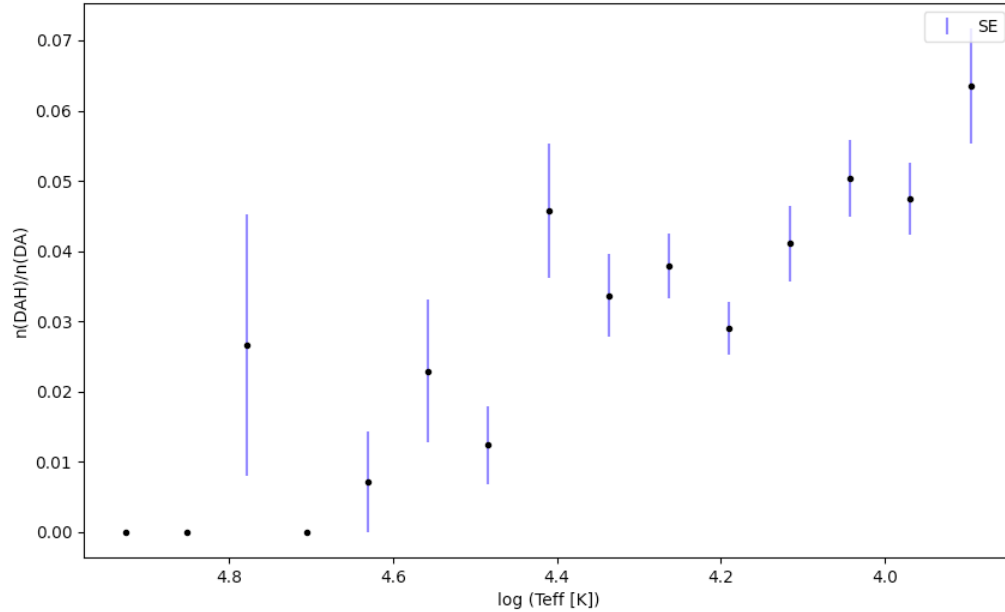


Figure 11. The ratio between the number of DAHs and the number of DAs versus effective temperature, showing a peak of abundance near $T_{\text{eff}} = 25\,000$ K. The blue vertical lines represent the standard errors for each point.

It is especially outstanding the rapid growth in magnetic fraction around effective temperature of $25\,000$ K ($\log T_{\text{eff}} \approx 4.4$), the temperature at which a convective zone of helium is internally formed in the white dwarf, that could be responsible for this increase. We also call attention to the build-up in the magnetic fraction that starts around the effective temperature of $16\,000$ K ($\log T_{\text{eff}} \approx 4.2$). At this temperature, a convective zone of hydrogen is formed in the white dwarf, and it could be responsible for the rise in the magnetic fraction.

A question then arises: does the effect change depending on the stellar mass? To answer this question, we divided our sample in two at $M = 0.8 M_{\odot}$ and at $M = 1 M_{\odot}$ and compared the results, which can be seen in the left and right panel of Figure 12 respectively.

The distribution with temperature of DAs doesn't change much, except for the fact that there are considerably fewer stars with $M > 1 M_{\odot}$. Differently, for the DAHs, there is a significant variation of the distribution. We highlight the valley around $10\,000$ K ($\log T_{\text{eff}} = 4.0$) as being a consequence of convective mixing and dilution. They pollute the stellar atmosphere with helium and thin the hydrogen layer, reducing the number of DAs and increasing the number of DABs or DBAs. This effect is constrained in temperature as a consequence of the disappearance of the lines of helium at lower temperatures, meaning that the star may contain helium in its atmosphere, it is only not possible to observe it through the spectra.

The magnetic DAs with mass above $0.8 M_{\odot}$ have a similar double peak behavior, even though it is more restricted in temperature. The magnetic DAs with mass above $1 M_{\odot}$ on the other hand have the second peak missing. Some mechanism must be inhibiting the magnetic field for higher masses at temperatures around $16\,000$ K ($\log T_{\text{eff}} \approx 4.2$). This same effect is not observed for masses below $1 M_{\odot}$. In fact, the opposite occurs, and they show the second peak much higher than the first. The behavior of the lower mass DAHs is precisely the one discussed earlier, thus becoming

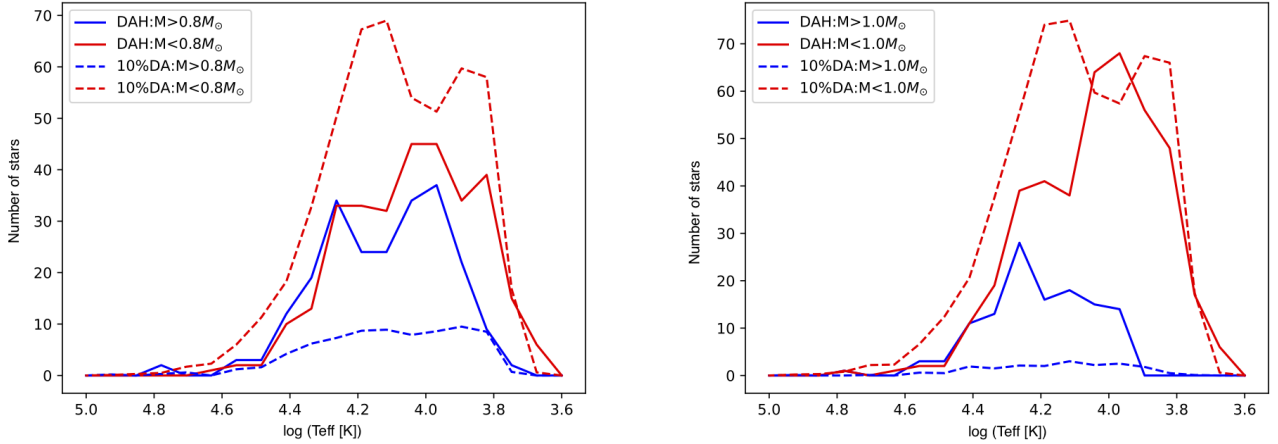


Figure 12. Both panels show the number of DAHs and DAs versus the effective temperature. The sample was divided at $0.8 M_{\odot}$ and $1.0 M_{\odot}$, represented in the upper panel and the lower panel respectively. We divided the absolute number of DAs by ten to allow better visualization. It is evident a change in behavior of the distribution of DAHs that is not accompanied by the distribution of DAs.

necessary the understanding of what could be suppressing the higher masses magnetic fields. It is valid to remember that more massive stars are usually less detected in magnitude limited samples because they are fainter, so this could also be the result of selection effects.

3.4. Relation between crystallization and magnetic field

One significant physical process that is highly dependent on the white dwarf mass is the crystallization of its core, and we suppose that it is the one holding the magnetic field back. In the search for a better understanding of the relation between the crystallization and the magnetic field, we built Figure 13, in which one can see not only if the star has started to crystallize its core but also have an idea of how advanced this process is. The further the star is from the crystallization line in the colder direction, the more crystallized its core is. We emphasize that the crystallization line has an intrinsic uncertainty to the models used to compute it.

It is recognizable that most of the stars with higher magnetic fields have started the crystallization process, which goes against the hypothesis that crystallization is responsible for the lower fraction of magnetic DAs with higher masses. Isern et al. (2017) proposed a mechanism of generation of magnetic fields of strengths of up to 0.1 MG by the dynamo in the convective region generated by the phase separation due to the crystallization process. Ginzburg et al. (2022) found that these fields could go as high as 100 MG depending on the rotational period of the star and its mass.

3.5. Particular Stars

Some stars have more than one spectrum observed by SDSS in which it is possible to look for variability in the line profiles as an indication of the rotational period. Besides the inclination of the star in respect to the line of sight, which may allow us to see different portions of the stellar surface as it rotates, the line profiles can also change due to the misalignment between the magnetic field axis and the rotation axis. Here we highlight the star SDSS J030407.40-002541.74 in which this effect is prominent. In Figure 14 we can see that the H_{α} line varies between a deeper central line to equally deep triplet components. It is also visible that the σ - component of the H_{β} line appears and disappears.

This star has also been observed by TESS, and we have 30 minutes cadence data from sectors 4 and 31. Unfortunately, no variation above the detection limit was identified, which is understandable since it is very faint (Gaia Mag = 17.8528).

The same process that affects the SDSS J030407.40-002541.74 H_{β} lines could be responsible for the H_{β} line profile of SDSS J221141.80+113604.5. which is illustrated in Figure 15. Kilic et al. (2021) argued that assuming a hydrogen atmosphere, an inclination, and an offset dipole geometry, the lines could not be reasonably reproduced. We found a good fit to the observed spectra except for the lateral components of the H_{β} line, which is expected to change as shown for SDSS J030407.40-002541.74.

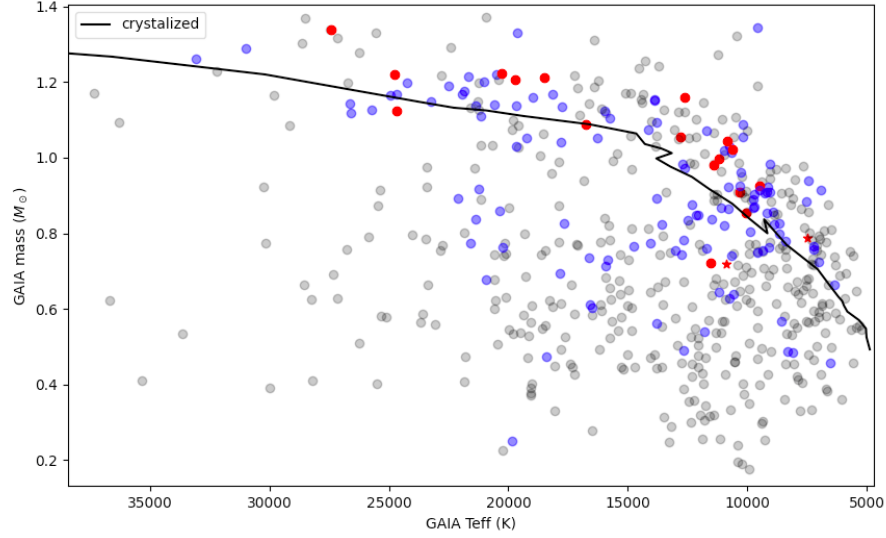


Figure 13. Mass versus effective temperature calculated with Gaia data. The colors black, blue, and red represent magnetic fields below 10 MG, between 10–100 MG, and above 100 MG, respectively. The two red stars represent the most magnetic DAs with a magnetic field above 700 MG. The solid black line represents the temperature of crystallization for the single evolution of white dwarfs of different masses as presented by Romero et al. (2013), Horowitz et al. (2010), and Lauffer et al. (2018). Crystallization increases to the right from the line, i.e., cooler temperatures.

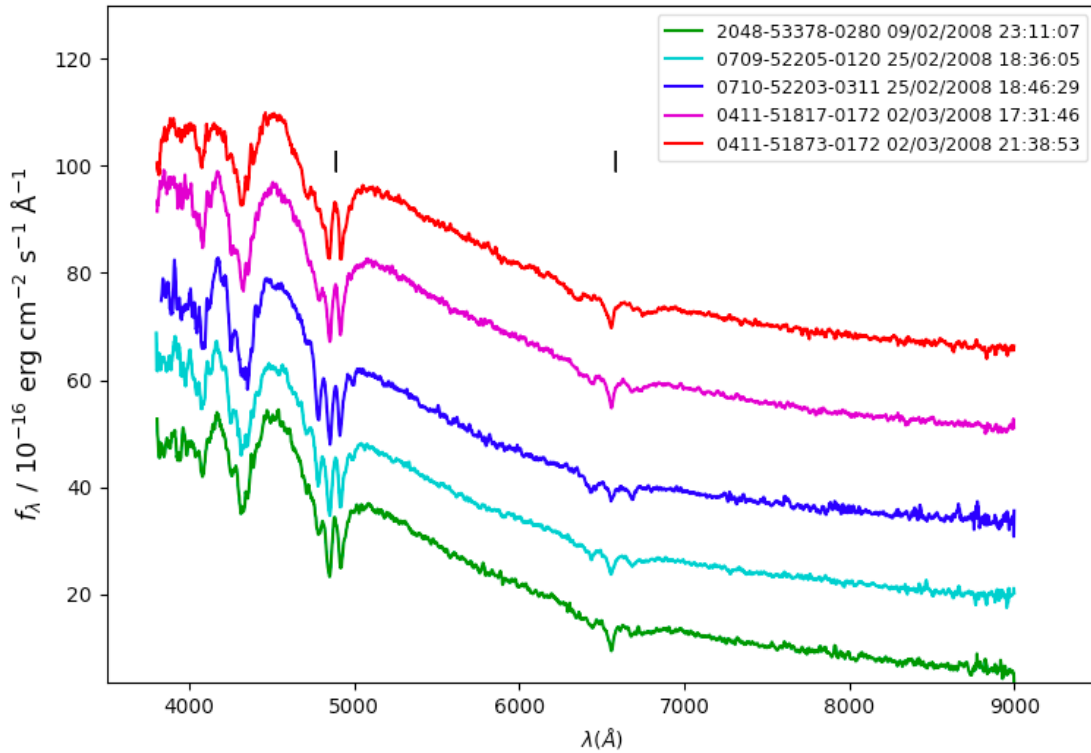


Figure 14. Different spectra of SDSS J030407.40-002541.74 with their respective observation dates. The two small vertical black segments mark the position of H_β and H_α lines.

Kilic et al. (2021) assumed a centered dipole as in Fig. 15 lower panel, and explained the difference in the line depth between the model and the observed spectra with the assumption of a non-pure hydrogen atmosphere. Our model does not require this additional complexity to explain the data.

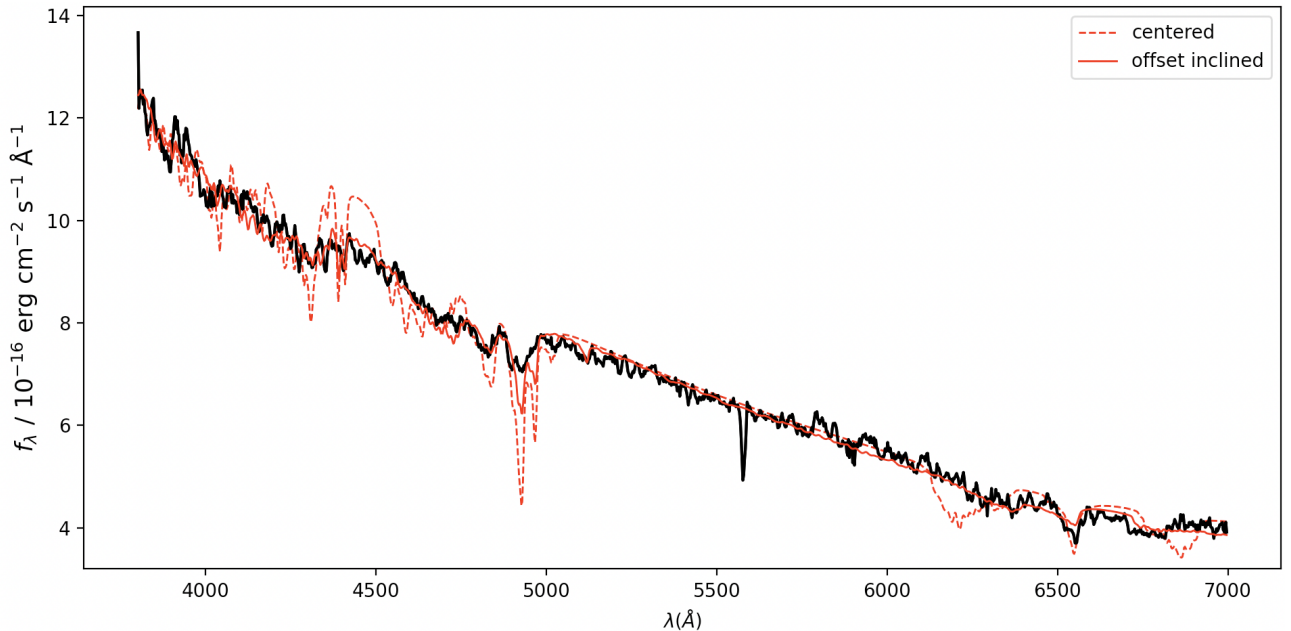


Figure 15. Observed spectrum of J221141.80+113604.5 with Plate-MJD-Fiber = 5064-55864-0122, $B=18.77$ MG, $S/N=20$ and $T_{\text{eff}} = 9500$ K. The model with the best least-squares fit to the data is shown in red. We highlight that the line near 5500 \AA is due to a systematic error of joining two different observations by SDSS. The full red line shows a model with computed offset magnetic dipole field geometry, while the dashed red line shows a model computed not inclined centered magnetic dipole field geometry with the strength found in the previous calculation.

Another interesting case is the star SDSS J225726.05+075541.6 featured in Williams et al. (2022). They stated that the observed Balmer lines are significantly weaker than predicted by the atmospheric models, which could be explained if the star were in an unresolved binary system, but the allowable parameter space for such a binary is minuscule. We found a good fit, again with only one component of H_{β} with large discrepancies. Our model is shown in Figure 16.

4. CONCLUSIONS

In this work, we estimated magnetic field strength for 804 white dwarfs observed from SDSS of which 287 are new discoveries. Save rare exceptions, our determinations are coherent with Kepler et al. (2013) and Külebi et al. (2009). It consists of the largest number of magnetic field determinations for white dwarfs to date. We searched for relations between magnetic field strength and stellar mass, effective temperature, and crystallization status.

It was found that a considerable percentage of DAH have fields below 3 MG. This is, to some extent, biased by our spectroscopic method, but could also mean that lower fields are more abundant in white dwarfs. This result is in opposition to Bagnulo & Landstreet (2021) which concluded that within the range of field strength found in the 20 pc volume, which extends between about 40 kG and 300 MG, the probability of fields occurring is roughly constant per dex of field strength.

We found that the magnetic field strength increases as the effective temperature decreases, together with an increase in the fraction of magnetic white dwarfs. This effect corroborates with the surface magnetic field being generated or enhanced in the white dwarf cooling phase. We could also observe that the highest fields tend to occur in the more massive stars and that the mean mass was, in general, higher than the non-magnetic ones ($0.78 M_{\odot}$ compared to the mean $0.6 M_{\odot}$). This does not give us any new information about the origin of the magnetic field because many assumptions already consider a higher mass. But a physical property closely related to the mass is crystallization, and we found that the most magnetic ones tend to be already crystallized. This is expected since DAH have higher masses,

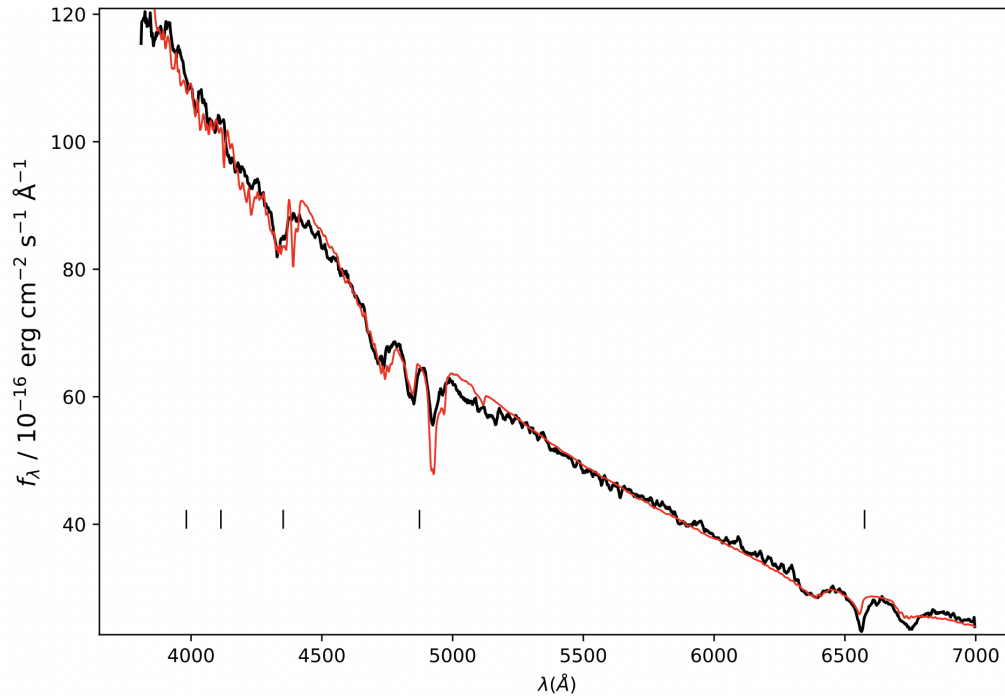


Figure 16. Observed spectrum of SDSS J225726.05+075541.6 with Plate-MJD-Fiber = 2310-53710-0420, $B=17.4$ MG, $S/N=34$ and $T_{\text{eff}} = 9500$ K. The model with the best least-squares fit to the data is shown in red.

so they crystallize at higher temperatures but spend more time (easier to detect) at lower temperatures (already crystallized).

The general behavior found in this work is compatible with the findings by [Bagnulo & Landstreet \(2022\)](#) that a high fraction of high-mass WDs have a strong magnetic field very early in their cooling phase, while normal mass stars are rarely magnetic when they are hot (young), but when they get cooler (older), magnetic fields become more common and stronger with time. Some other mechanism may be inhibiting magnetic fields in WDs with $M \geq 1 M_{\odot}$ and $T_{\text{eff}} \leq 16000$ K.

1 We thank the support by grants from CAPES and CNPq (Brazil).

Facilities: SDSS [Kepler et al. \(2021\)](#), Gaia [Gentile Fusillo et al. \(2021\)](#).

Software: [astropy \(Astropy Collaboration et al. 2013, 2018\)](#), [YAWP Külebi et al. \(2009\)](#).

APPENDIX

A. COMPLETE TABLE

Table 2. The table presents the identifiers of the DAHs in the SDSS and their masses and effective temperatures calculated with Gaia astrometry presented in [Gentile Fusillo et al. \(2021\)](#) when available. Then we have the temperature used for the magnetic field model, computed using non-magnetic atmospheric models and SDSS colors g, r, and i. The following columns present the parameters of the magnetic field resulting from the best YAWP model for each star. In order, there is the dipole magnetic field strength of the offset dipole, the uncertainty computed through least squares, the z-offset from the center, and the inclination of the dipole to the line of sight. We call attention that these last two quantities should be interpreted as a reference for the magnetic field structure because there are many degeneracies for the geometry.

SDSS	Plate-MJD-Fiber	M	T _{eff}	T _{SDSS}	B	$\sigma(B)$	z _{offset}	incl
		(M _⊙)	(K)	(K)	(MG)	(MG)	(R _*)	(°)
J113212.99-003036.8	0282-51658-0278	—	—	20000	3.19	0.46	0.04	21.79
J114720.40-002405.7	0283-51584-0120	0.68	15919	17000	2.00	—	—	33.47
J121105.25-004628.5	0287-52023-0253	1.34	27473	19500	2.56	0.01	-0.32	66.65
J121635.36-002656.3	0288-52000-0276	—	—	15000	64.24	0.11	-0.18	59.27
J130807.48-010117.0	0294-51986-0089	0.47	11757	18500	2.20	0.00	-0.21	72.94
J144114.21+003702.3	0307-51663-0595	0.87	25472	21000	4.39	0.49	0.49	20.70
J112852.88-010540.7	0326-52375-0565	—	—	18000	2.81	0.36	0.36	0.08
J113431.97-031529.0	0327-52294-0131	1.24	14539	15500	3.00	0.01	0.34	16.44
J155238.20+003910.4	0342-51691-0639	1.26	14285	12500	2.16	0.08	0.12	41.32
J171556.26+600643.7	0354-51792-0318	0.55	13567	9500	2.07	0.01	0.17	27.63
J172932.48+563204.1	0358-51818-0239	—	—	10000	6.00	0.04	0.49	0.46
J172329.14+540755.7	0359-51821-0415	1.09	10175	10000	36.82	6.75	-0.05	53.78
J173915.64+545059.1	0360-51816-0547	0.30	9376	16000	2.69	0.02	0.37	31.91
J173235.19+590533.3	0366-52017-0591	0.57	11028	11500	2.56	0.04	-0.36	78.63
J171441.07+552711.3	0367-51997-0318	—	—	30000	6.45	1.80	0.47	3.84
J172045.35+561214.8	0367-51997-0461	—	—	15000	24.67	0.01	-0.30	78.71
J220435.05+001242.9	0372-52173-0626	1.11	10502	10500	2.15	0.00	0.13	12.83
J220823.65-011534.1	0373-51788-0086	0.39	19044	9500	3.04	0.11	-0.50	35.80
J220514.08-005841.6	0373-51788-0243	0.75	18464	14500	3.01	0.02	0.42	74.80
J221828.58-000012.1	0374-51791-0583	1.06	12806	12239	220.78	6.35	-0.04	24.85
J231432.89-011320.3	0382-51816-0289	—	—	18500	4.50	0.00	0.45	4.02
J232248.21+003901.0	0383-51818-0421	1.17	18130	11500	21.20	0.49	-0.38	33.30
J022335.15+004954.8	0406-51900-0490	0.54	6728	9500	2.16	0.02	-0.15	65.68
J022523.67+002743.0	0406-51900-0543	—	—	15500	2.02	0.00	0.16	0.16
J022623.80-002313.1	0406-52238-0071	—	—	16500	1.30	0.12	0.00	33.47
J025837.19+000019.2	0410-51877-0065	0.75	10561	10000	2.33	0.01	0.16	2.51
J032137.43+010437.3	0413-51821-0578	0.89	21140	18000	2.86	0.00	0.05	16.68
J031323.65-001659.9	0413-51929-0313	—	—	30000	7.30	0.00	0.42	0.00
J033145.69+004516.9	0415-51879-0378	1.05	19230	12000	13.05	2.37	-0.42	48.36
J033320.37+000720.6	0415-51879-0485	0.79	7498	9500	771.71	214.35	0.18	0.10
J034511.10+003444.2	0416-51811-0590	0.57	7431	8000	2.50	0.27	-0.36	12.91
J003111.75+134919.5	0417-51821-0084	—	—	21000	2.24	0.00	0.15	0.72
J003232.07+153126.6	0418-51817-0346	0.35	9917	17000	2.00	0.78	0.10	15.36

Table 2 continued on next page

Table 2 (continued)

SDSS	Plate-MJD-Fiber	M	T _{eff}	T _{SDSS}	B	$\sigma(B)$	Z _{offset}	incl
		(M _⊙)	(K)	(K)	(MG)	(MG)	(R _*)	(°)
J004513.88+142248.1	0419-51879-0147	0.81	7629	8000	3.61	0.04	-0.29	18.68
J013533.20+132249.8	0426-51882-0291	—	—	21000	5.10	0.01	0.00	33.47
J013920.54+152218.7	0426-51882-0524	0.46	10530	18000	2.30	0.00	0.19	0.56
J021230.00+122557.2	0428-51883-0046	—	—	15500	2.07	0.11	0.14	0.80
J075959.57+433521.1	0437-51869-0369	—	—	9000	91.55	57.78	-0.38	29.35
J081136.33+461156.4	0439-51877-0523	—	—	40000	4.95	2.77	0.49	3.90
J085159.32+532540.3	0449-51900-0311	0.87	11106	11500	63.76	28.16	-0.17	13.81
J093921.25+581421.4	0452-51911-0553	—	—	21000	2.40	0.01	0.19	18.17
J094046.28+595415.8	0453-51915-0325	0.19	10231	12000	2.04	0.00	0.21	2.05
J023609.43-080823.7	0455-51909-0474	—	—	10500	34.00	0.12	0.29	11.01
J031630.64-081529.1	0459-51924-0002	0.55	9556	9500	2.19	0.01	-0.23	65.04
J032404.30-061756.5	0460-51924-0525	0.65	7653	8000	3.03	0.31	-0.50	43.37
J034240.63-073504.0	0462-51909-0084	—	—	19500	2.13	0.64	0.06	5.54
J034308.17-064127.3	0462-51909-0117	1.07	14130	12000	11.43	0.00	-0.50	20.09
J041209.32-054031.0	0465-51910-0017	0.85	12121	12000	32.61	0.23	-0.22	6.48
J090343.13+011846.3	0470-51929-0403	—	—	11000	3.10	0.12	0.00	33.47
J092242.42+011422.8	0473-51929-0003	—	—	30000	8.50	0.00	-0.28	23.97
J092527.46+011328.6	0475-51965-0315	0.91	10390	10500	3.05	0.08	-0.47	56.99
J094012.88-000009.9	0476-52314-0597	0.43	17240	24000	2.58	0.12	0.22	18.30
J094945.34+003619.1	0480-51989-0045	—	—	9500	3.00	0.00	0.38	0.33
J094711.11+003754.6	0480-51989-0082	1.06	14898	9000	2.56	0.00	0.21	89.92
J094351.25+010104.0	0480-51989-0251	—	—	9500	2.19	erro	-0.20	89.08
J084937.77+561949.1	0483-51902-0296	0.70	9831	15000	2.47	0.01	0.18	4.88
J085309.08+563441.5	0483-51924-0203	0.50	7077	10000	1.10	0.03	0.00	33.47
J104356.63+650057.2	0489-51930-0079	1.03	13856	18000	4.10	0.03	0.00	33.47
J104012.21+660520.1	0489-51930-0535	1.19	9557	9500	2.49	0.02	-0.35	59.34
J105628.48+652313.4	0490-51929-0205	0.49	12667	18000	23.21	0.01	-0.10	54.56
J111150.80+663736.2	0490-51929-0639	0.49	16191	23000	5.50	—	—	33.47
J121557.40+665344.5	0493-51957-0104	—	—	8000	2.73	0.35	-0.35	5.79
J100005.66+015859.0	0500-51994-0557	—	—	17000	25.52	0.11	0.31	2.06
J100732.63+010914.6	0501-52235-0004	—	—	9000	2.47	0.43	0.34	38.75
J100822.39+015307.4	0501-52235-0077	—	—	40000	3.85	0.00	0.47	4.24
J101206.88+022003.1	0502-51957-0495	—	—	8000	2.20	0.01	0.19	20.12
J101805.04+011123.4	0503-51999-0244	0.91	10329	11000	122.69	15.97	0.01	65.25
J105332.61+020126.2	0507-52353-0113	0.36	6024	8000	2.54	0.11	-0.36	42.75
J115418.14+011711.5	0515-52051-0126	1.12	26581	18000	37.35	13.80	-0.31	79.10
J121209.31+013627.7	0518-52282-0285	0.64	10554	10500	10.97	0.84	-0.49	45.46
J144649.26+005215.3	0537-52027-0126	—	—	18500	2.10	0.00	0.17	0.80
J144408.75+024327.8	0537-52027-0371	0.33	7772	10500	2.50	0.02	-0.11	24.11
J144934.72+025502.7	0537-52027-0566	0.71	8899	8000	3.61	0.02	-0.49	4.25

Table 2 continued on next page

Table 2 (continued)

SDSS	Plate-MJD-Fiber	M	T _{eff}	T _{SDSS}	B	$\sigma(B)$	Z _{offset}	incl
		(M _⊙)	(K)	(K)	(MG)	(MG)	(R _*)	(°)
J150220.91+001721.1	0539-52017-0202	0.48	7440	10000	2.20	0.02	0.00	33.47
J074947.00+354055.4	0542-51993-0639	1.33	19628	39100	30.00	0.16	0.23	6.68
J080743.33+393829.1	0545-52202-0009	—	—	20000	38.00	0.17	0.26	11.63
J082159.66+431127.3	0547-52207-0019	—	—	22000	1.70	0.01	0.00	33.47
J092932.55+561318.4	0556-51991-0326	0.33	7291	9000	2.26	0.38	0.18	7.67
J095211.45+563020.7	0557-52253-0170	0.57	19045	22652	2.01	0.00	0.07	69.66
J095919.86+573542.9	0558-52317-0158	—	—	17500	5.08	0.02	0.15	7.35
J105404.37+593333.1	0561-52295-0008	0.49	8316	15500	18.10	—	—	33.47
J084155.73+022350.5	0564-52224-0248	0.78	6942	8000	3.67	0.23	-0.28	9.81
J093508.56+042116.7	0569-52264-0452	—	—	19500	1.30	0.01	0.00	33.47
J094103.84+032835.8	0570-52266-0279	—	—	25000	1.80	—	—	33.47
J094815.26+041648.6	0570-52266-0632	—	—	16500	3.30	0.18	0.36	0.16
J101618.37+040920.5	0574-52355-0166	—	—	12500	4.05	0.06	0.17	30.28
J105709.81+041130.3	0580-52368-0274	0.71	8330	8000	2.77	0.19	-0.34	41.45
J142955.20+044005.4	0585-52027-0467	1.31	16401	12500	2.57	0.02	-0.38	67.92
J145029.51+032218.8	0587-52026-0016	1.08	19587	22000	2.65	0.00	0.18	5.70
J145801.09+040917.0	0588-52029-0639	—	—	16500	3.19	0.01	0.47	13.25
J154135.01+030051.1	0594-52045-0253	—	—	13500	3.60	0.02	0.00	33.47
J154120.14+022756.5	0594-52045-0315	0.53	19164	23000	3.21	0.18	0.12	14.85
J154213.46+034800.3	0594-52045-0400	1.05	10586	9500	8.58	0.17	-0.19	46.30
J112022.01+635437.4	0597-52059-0308	0.64	7248	9500	3.24	0.69	0.47	6.99
J133340.34+640627.3	0603-52056-0112	1.12	12859	9500	7.25	0.19	-0.05	13.97
J144614.00+590216.6	0608-52081-0140	—	—	16000	10.21	0.07	0.31	21.27
J145636.32+583321.1	0610-52056-0189	0.47	7226	9500	2.47	1.20	-0.35	54.75
J151745.18+610543.6	0613-52345-0446	—	—	15000	23.79	0.09	0.36	0.68
J153301.51+550840.9	0614-53437-0079	0.62	8804	9500	3.60	0.05	0.00	33.47
J153315.25+564200.2	0614-53437-0579	0.75	9916	11000	2.50	—	—	33.47
J160437.35+490809.2	0622-52054-0330	0.86	8932	9000	37.97	15.25	-0.15	13.42
J162727.70+492507.9	0625-52145-0578	0.65	7999	11000	1.10	0.01	0.00	33.47
J204626.15-071036.9	0635-52145-0227	0.76	8388	8000	2.58	0.24	-0.4	46.19
J214930.73-072811.9	0644-52173-0350	0.84	21374	23000	40.98	15.09	-0.07	76.42
J234623.68-102356.9	0648-52559-0142	0.76	8644	9500	3.00	0.07	-0.32	13.84
J004122.49-110432.5	0655-52162-0091	0.81	6770	8000	2.44	0.27	-0.37	11.19
J010654.65-104315.1	0659-52199-0207	—	—	8500	2.81	0.22	-0.19	54.68
J224742.57-003317.4	0676-52178-0319	—	—	30000	5.13	25.63	0.50	3.81
J225230.63+003232.6	0676-52178-0481	—	—	30000	5.20	1.99	0.49	10.01
J230758.83+000500.4	0678-52884-0498	—	—	22000	3.12	0.01	0.08	14.96
J230904.69+001803.0	0678-52884-0547	—	—	8000	2.98	0.06	-0.42	67.79
J233328.29-002036.6	0682-52525-0317	—	—	11000	2.70	0.01	0.00	33.47
J234710.26+000633.4	0683-52524-0520	0.97	8797	9500	6.00	0.10	0.39	5.76

Table 2 continued on next page

Table 2 (*continued*)

SDSS	Plate-MJD-Fiber	M	T _{eff}	T _{SDSS}	B	$\sigma(B)$	Z _{offset}	incl
		(M _⊙)	(K)	(K)	(MG)	(MG)	(R _*)	(°)
J004248.20+001955.2	0690-52261-0594	—	—	14000	8.50	0.19	0.37	23.32
J010225.13-005458.6	0693-52254-0099	1.33	25533	22000	2.70	0.55	-0.01	2.89
J014938.34-004938.0	0699-52202-0012	0.80	24023	16000	3.26	0.01	0.48	4.02
J015748.19-010600.9	0701-52179-0291	0.72	7228	8000	2.73	0.01	0.22	1.98
J030417.87-003216.4	0709-52205-0107	0.36	8452	14000	4.29	2.77	0.49	12.73
J032300.93+002221.4	0712-52199-0427	—	—	14500	2.70	—	—	33.47
J213819.85+112311.3	0731-52460-0632	0.59	9561	9500	2.19	0.15	-0.39	3.17
J215148.31+125525.2	0733-52207-0522	—	—	10000	20.71	0.26	-0.17	66.83
J224103.29+132853.2	0739-52520-0143	—	—	23000	2.15	0.00	0.16	27.51
J002128.59+150223.7	0753-52233-0432	0.73	7019	9000	76.49	77.59	-0.46	20.21
J075819.57+354443.6	0757-52238-0144	1.14	19664	15000	25.68	5.71	-0.4	20.02
J075842.68+365731.5	0757-52238-0439	0.39	6688	8000	1.10	0.06	0.00	33.47
J080938.10+373053.8	0758-52253-0044	0.83	12497	11398	46.42	0.21	-0.10	55.43
J082533.22+412400.1	0760-52264-0640	0.66	28554	23000	2.27	0.00	0.08	9.63
J095603.30+540907.0	0769-54530-0078	0.50	11319	14000	3.51	0.01	0.05	4.99
J114006.38+611008.1	0776-52319-0042	0.83	17686	13000	65.78	0.21	-0.03	68.25
J120803.25+625815.3	0778-54525-0511	0.51	26238	40000	3.35	0.00	0.49	10.42
J134017.70+594552.5	0786-52319-0254	0.41	35350	35770	2.60	0.02	-0.36	77.51
J143632.86+563525.2	0791-52435-0304	0.50	6478	8500	1.10	0.03	0.00	33.47
J153829.29+530604.6	0795-52378-0637	1.11	21158	9500	16.12	0.04	0.12	61.27
J155857.29+480047.3	0813-52354-0328	1.07	11406	10000	2.42	0.01	0.25	81.07
J160929.96+443857.1	0814-52370-0317	—	—	30000	1.50	0.11	0.00	33.47
J165203.67+352815.7	0820-52438-0299	0.63	10756	18778	10.62	0.30	0.20	76.02
J085830.85+412635.0	0830-52293-0070	—	—	8000	2.20	0.08	-0.08	45.68
J081130.20+305720.4	0861-52318-0096	0.43	11857	9000	2.50	0.15	-0.18	47.00
J084226.97+374040.1	0864-52320-0524	0.45	12069	9500	2.78	0.21	-0.36	60.38
J105328.13+505155.2	0876-52669-0510	0.89	8090	9000	2.82	0.02	-0.44	56.93
J113357.65+515204.6	0879-52365-0586	1.22	22816	22000	9.67	1.55	-0.35	80.00
J123204.19+522548.2	0885-52379-0319	0.45	8391	8183	8.16	0.04	-0.13	37.40
J074853.07+302543.5	0889-52663-0507	1.17	37325	28932	8.15	1.46	0.02	35.96
J081018.72+370010.9	0892-52378-0374	0.77	9926	9556	2.50	1.29	-0.31	80.65
J093447.89+503312.1	0901-52641-0373	0.77	8536	8946	6.61	0.52	-0.10	41.23
J100932.74+524638.2	0903-52400-0584	1.16	14442	15122	2.28	0.11	-0.28	81.23
J145602.52-005548.7	0921-52380-0528	0.49	17807	20000	2.10	—	—	33.47
J152855.62-015148.7	0925-52411-0312	—	—	19500	2.40	0.00	0.18	0.31
J082239.54+304857.1	0931-52619-0078	—	—	17500	2.40	0.08	0.00	33.47
J085130.57+353117.6	0934-52672-0080	0.62	6548	8000	2.50	0.21	-0.07	15.82
J091856.12+411317.9	0938-52708-0413	—	—	9500	2.78	0.17	0.31	87.79
J112926.23+493931.8	0966-52642-0474	0.65	9929	10000	3.05	0.23	-0.50	19.54
J113408.25+485601.8	0967-52636-0319	—	—	40000	2.77	0.07	-0.41	60.03

Table 2 *continued on next page*

Table 2 (continued)

SDSS	Plate-MJD-Fiber	M	T _{eff}	T _{SDSS}	B	$\sigma(B)$	Z _{offset}	incl
		(M _⊙)	(K)	(K)	(MG)	(MG)	(R _*)	(°)
J170400.00+321328.5	0976-52413-0319	—	—	25000	3.44	0.01	0.49	5.16
J171831.24+280825.6	0980-52431-0434	—	—	30000	3.01	0.38	0.43	18.20
J205233.51-001610.6	0982-52466-0019	1.17	21947	18500	15.15	0.23	-0.37	60.48
J214539.83+000136.5	0990-52465-0080	—	—	25000	1.80	0.95	0.00	33.47
J101420.37+060254.0	0996-52641-0025	—	—	19000	2.30	0.01	0.00	33.47
J105216.00+530120.3	1010-52649-0597	—	—	19500	2.44	0.05	0.18	0.05
J093200.38+350429.8	10244-58225-0112	—	—	9500	2.19	0.01	-0.22	81.50
J073819.64+282126.9	10285-58083-0155	0.58	8447	8000	2.73	0.17	-0.34	60.56
J144345.84+482008.9	1047-52733-0099	0.80	19328	22000	2.02	0.01	0.12	36.94
J153532.25+421305.5	1052-52466-0252	—	—	22000	2.80	0.01	0.00	33.47
J153742.29+434719.7	1052-52466-0619	—	—	40000	2.86	2.62	0.24	0.85
J161030.50+365442.3	1056-52764-0440	1.22	17214	23000	2.16	0.07	0.19	27.22
J090451.92+293755.0	10667-58163-0282	—	—	13000	5.35	0.10	-0.50	52.99
J222313.51+005446.5	1103-52873-0531	—	—	8000	2.77	0.01	-0.35	58.97
J220524.60+010503.3	1105-52937-0404	1.05	12457	19000	2.49	0.01	-0.17	73.94
J214900.86+004842.7	1107-52968-0374	1.22	20497	16000	11.04	—	—	67.43
J014032.41+090520.3	11070-58452-0012	—	—	10500	4.25	0.33	0.46	22.12
J080724.47+260238.3	11121-58438-0361	—	—	22000	8.19	0.05	-0.25	27.61
J082141.04+264800.7	11125-58433-0906	0.75	13230	15500	3.02	0.18	-0.43	50.15
J232353.30+060715.7	11294-58451-0284	—	—	8000	15.12	0.10	0.06	60.40
J165249.08+333444.9	1175-52791-0095	0.53	8118	8500	4.58	0.10	-0.12	57.86
J165029.90+341125.4	1175-52791-0482	0.89	9842	10500	3.05	0.02	-0.50	43.28
J081648.70+041223.5	1184-52641-0329	—	—	15000	11.10	—	—	33.47
J082231.16+033113.7	1184-52641-0637	0.67	7936	8000	4.18	0.06	-0.23	58.73
J084910.12+044528.7	1188-52650-0635	—	—	15000	2.49	0.00	0.35	6.48
J084628.04+064532.8	1189-52668-0344	—	—	23000	1.30	—	—	33.47
J091437.35+054453.3	1193-52652-0481	1.03	20681	23420	9.23	8.77	-0.08	66.59
J091314.47+410838.6	1200-52668-0079	—	—	19000	3.56	1.63	0.38	6.96
J094458.92+453901.1	1202-52672-0577	1.04	17775	20000	15.42	0.08	0.16	63.31
J082835.81+293448.6	1207-52672-0635	0.89	13786	25000	33.43	0.17	0.15	36.11
J090746.83+353821.5	1212-52703-0187	1.05	16269	19000	19.13	0.13	0.25	5.87
J093409.90+392759.3	1215-52725-0241	0.71	9294	10985	3.08	0.13	-0.49	50.00
J110735.31+085924.5	1221-52751-0177	1.18	17097	18997	2.64	0.08	-0.26	56.98
J111812.67+095241.3	1222-52763-0477	0.98	11398	14306	2.27	0.05	-0.30	54.84
J112328.48+095619.4	1222-52763-0625	0.75	9356	9000	2.25	0.05	-0.30	63.16
J101529.62+090703.7	1237-52762-0533	0.77	7102	8000	2.51	0.25	-0.37	2.59
J104113.69+083505.2	1240-52734-0105	—	—	25000	4.04	1.33	0.48	3.98
J090623.50+332108.0	1272-52989-0519	0.66	13739	18500	3.25	0.02	0.47	4.08
J093411.36+364641.2	1275-52996-0174	—	—	10500	2.23	0.06	-0.29	59.76
J145414.99+432149.4	1290-52734-0469	0.89	11400	11500	3.26	0.05	-0.50	45.85

Table 2 continued on next page

Table 2 (continued)

SDSS	Plate-MJD-Fiber	M	T _{eff}	T _{SDSS}	B	$\sigma(B)$	Z _{offset}	incl
		(M _⊙)	(K)	(K)	(MG)	(MG)	(R _*)	(°)
J153057.48+394614.8	1293-52765-0613	—	—	25000	2.20	0.01	0.50	3.65
J083745.12+064313.8	1297-52963-0637	0.76	26780	30000	4.76	0.35	0.39	15.76
J090632.65+080715.9	1300-52973-0148	1.17	14359	40000	7.55	0.18	-0.35	29.15
J091005.44+081512.2	1300-52973-0639	0.63	27176	30000	2.42	1.29	0.11	2.24
J091220.25+075537.7	1301-52976-0241	—	—	15500	2.30	0.29	0.19	20.22
J093356.39+102215.6	1303-53050-0525	0.40	7680	9075	2.58	0.23	-0.38	54.90
J113756.50+574022.4	1311-52765-0421	0.68	7507	10080	5.00	0.15	-0.17	13.73
J125415.99+561204.6	1318-52781-0299	0.86	10773	11500	82.60	0.41	0.39	13.29
J135141.13+541947.2	1323-52797-0293	0.72	10858	10180	778.51	0.00	0.16	20.40
J142118.19+523547.0	1326-52764-0250	—	—	25000	2.77	0.70	0.24	15.78
J155436.25+413956.6	1334-52764-0235	0.54	11795	23000	13.14	0.08	0.31	14.28
J163841.66+334302.1	1339-52767-0092	—	—	9500	2.19	0.06	-0.20	70.44
J120728.95+440731.6	1369-53089-0048	0.54	15397	19000	2.16	0.01	0.12	32.10
J143218.25+430126.7	1396-53112-0338	0.59	23596	30000	2.65	0.02	-0.01	43.03
J144541.71+411441.5	1397-53119-0352	—	—	21000	4.29	0.84	0.49	3.68
J150813.26+394505.1	1398-53146-0633	—	—	29032	6.40	1.11	-0.21	25.68
J154305.66+343223.6	1402-52872-0145	1.16	29802	30620	4.98	0.12	0.47	81.04
J160246.45+303914.5	1405-52826-0283	0.39	29982	40000	3.55	0.68	0.36	8.92
J164357.02+240201.3	1414-53135-0191	0.61	19026	23000	2.47	1.59	0.01	1.02
J155651.96+351218.9	1417-53141-0512	0.57	7515	8000	3.07	0.10	-0.50	46.10
J103635.00+391814.0	1430-53002-0078	—	—	8000	2.80	0.12	0.25	83.93
J104136.43+404317.8	1432-53003-0522	—	—	8000	2.73	0.03	-0.35	9.29
J112714.82+411737.6	1443-53055-0302	0.58	7003	8000	3.05	0.08	-0.48	42.64
J114852.77+430753.1	1447-53120-0323	—	—	40000	2.30	0.00	0.24	6.23
J122249.13+481133.1	1451-53117-0582	0.78	9053	9000	9.71	0.30	-0.34	77.45
J122401.47+415551.9	1452-53112-0181	0.91	9185	10000	23.65	1.21	-0.28	58.89
J124806.37+410427.1	1456-53115-0190	0.73	7258	8000	4.80	0.22	-0.21	7.04
J130214.98+415726.0	1458-53119-0490	1.24	13707	17000	2.88	0.01	0.24	34.29
J133828.43+415943.8	1464-53091-0605	0.45	12333	17500	3.24	0.66	0.46	14.23
J140821.99+443008.0	1467-53115-0557	0.30	12368	12500	3.20	0.01	0.47	7.70
J010214.99+462620.9	1472-52913-0278	—	—	8033	2.58	0.15	-0.38	53.48
J164626.65+222645.4	1570-53149-0615	0.97	14822	14000	2.11	0.01	0.12	1.40
J162808.39+233254.1	1573-53226-0099	0.78	7325	8000	4.77	0.21	-0.21	18.64
J080150.49+205012.0	1583-52941-0599	—	—	19000	2.18	0.00	0.17	22.86
J080502.28+215320.5	1584-52943-0132	—	—	37141	6.77	0.17	-0.49	66.27
J084008.49+271242.6	1587-52964-0059	0.82	10948	12500	11.19	0.36	-0.44	69.48
J084929.10+285720.3	1588-52965-0565	1.09	13796	15500	28.00	0.77	0.17	12.57
J101519.32+114724.1	1597-52999-0531	—	—	11500	2.77	0.00	-0.37	76.73
J123414.11+124829.5	1616-53169-0423	0.45	8053	8544	2.26	0.58	-0.50	1.88
J115554.94+083549.5	1622-53385-0447	0.74	8385	9888	3.04	0.10	-0.46	59.81

Table 2 continued on next page

Table 2 (continued)

SDSS	Plate-MJD-Fiber	M	T _{eff}	T _{SDSS}	B	$\sigma(B)$	Z _{offset}	incl
		(M _⊙)	(K)	(K)	(MG)	(MG)	(R _*)	(°)
J120609.81+081323.7	1623-53089-0573	0.86	10057	16000	449.10	35.47	0.01	51.31
J152934.98+292801.8	1652-53555-0436	0.96	11097	10000	2.82	0.29	-0.44	67.06
J161118.59+242446.6	1657-53520-0372	0.53	8361	11000	1.30	0.04	0.0	33.47
J203828.47+764123.1	1661-53240-0023	0.48	12071	16000	2.16	0.23	0.15	14.78
J203016.12+765022.6	1661-53240-0116	—	—	14000	3.04	0.02	0.07	25.19
J201822.88+754807.6	1661-53240-0124	—	—	14500	2.61	1.56	0.21	6.60
J232937.54+524437.8	1663-52973-0119	0.59	17226	32204	2.24	0.05	-0.31	74.89
J132538.57+515152.2	1668-53433-0326	—	—	10000	3.15	0.01	0.45	13.00
J141808.12+481850.6	1672-53460-0181	0.32	11963	13000	2.28	0.04	-0.32	73.22
J151102.74+433558.7	1677-53148-0151	—	—	13000	2.19	0.00	0.14	2.10
J153554.17+404414.2	1679-53149-0109	—	—	30000	2.39	0.01	0.22	6.36
J170657.89+232118.9	1687-53260-0019	0.37	19077	24000	3.31	0.30	0.09	17.17
J170916.36+234111.3	1688-53462-0508	0.41	7874	18500	4.27	0.31	0.19	33.14
J165538.92+253346.2	1692-53473-0163	—	—	15500	2.76	4.34	0.32	39.02
J165354.57+251738.4	1692-53473-0213	—	—	19000	1.20	—	—	33.47
J170019.41+245701.3	1693-53446-0169	—	—	30000	2.02	0.00	0.18	25.83
J124819.86+133555.5	1694-53472-0564	1.03	19582	13000	2.14	0.01	-0.25	82.57
J133007.57+104830.5	1699-53148-0137	0.57	7172	8000	2.16	0.08	-0.09	47.51
J143308.49+102623.0	1709-53533-0511	0.78	6698	8000	2.49	0.22	-0.37	18.51
J153843.10+084238.2	1725-54266-0297	0.91	9060	33803	12.66	0.27	0.03	43.78
J155932.57+081904.6	1728-53228-0175	0.40	10187	13000	1.30	0.01	0.00	33.47
J155651.11+085003.5	1728-53228-0374	0.67	10515	10500	2.19	0.04	-0.14	74.13
J160852.00+064437.0	1730-53498-0252	0.83	8655	8500	24.86	0.14	-0.24	73.69
J161658.43+070355.4	1731-53884-0442	—	—	12500	3.19	0.44	0.46	25.95
J162115.34+075059.0	1732-53501-0455	0.81	14816	12000	2.19	0.01	0.29	34.17
J090150.74+091211.4	1738-53051-0002	0.66	9219	11000	2.67	0.12	-0.35	55.18
J100715.55+123709.4	1745-53061-0313	0.80	21864	23000	5.08	1.55	0.11	0.87
J080719.89+064536.6	1756-53080-0234	—	—	21000	2.14	0.11	0.15	17.84
J081144.59+071030.5	1756-53080-0585	0.60	16080	17000	2.13	0.00	0.13	2.79
J082239.43+082436.7	1758-53084-0346	0.91	10039	10500	2.57	0.18	-0.35	69.08
J083002.71+083631.9	1758-53084-0531	0.68	15378	12500	3.01	0.00	0.44	18.55
J084253.04+092226.5	1759-53081-0618	0.39	12670	11500	3.40	0.08	0.05	5.39
J115345.96+133106.6	1762-53415-0042	0.55	12173	19000	2.45	—	—	33.47
J114827.96+153356.9	1762-53415-0372	—	—	16000	2.17	0.56	0.15	1.85
J120806.25+144942.8	1764-53467-0112	—	—	18000	4.70	0.02	0.00	33.47
J123527.08+145318.6	1768-53442-0074	0.25	13281	16500	2.06	0.02	0.11	22.21
J123449.88+150348.8	1768-53442-0557	0.69	6125	8000	8.22	0.30	-0.06	5.68
J125044.42+154957.3	1770-53171-0530	0.48	8073	10000	21.51	1.66	-0.42	40.30
J125553.38+152555.0	1771-53498-0343	0.47	18411	22000	12.88	0.05	0.26	33.17
J131050.04+143520.4	1772-53089-0559	—	—	40000	4.15	0.00	0.48	2.18

Table 2 continued on next page

Table 2 (continued)

SDSS	Plate-MJD-Fiber	M	T _{eff}	T _{SDSS}	B	$\sigma(B)$	Z _{offset}	incl
		(M _⊙)	(K)	(K)	(MG)	(MG)	(R _*)	(°)
J132002.47+131901.5	1773-53112-0011	0.20	10388	21000	3.17	0.96	0.04	4.27
J155620.60+055029.4	1822-53172-0139	—	—	8000	42.00	0.01	0.27	18.87
J155857.68+041704.8	1837-53494-0261	0.91	6912	8000	69.82	15.31	-0.16	9.63
J135654.77+343617.2	1838-53467-0240	—	—	30000	9.30	2.32	0.50	2.96
J151625.06+280320.9	1846-54173-0280	0.64	7877	8000	2.30	0.07	0.00	33.47
J154605.40+243759.0	1850-53786-0312	0.74	6327	8000	1.10	0.11	0.00	33.47
J155657.69+231358.5	1851-53524-0298	0.47	19183	13000	3.27	0.05	0.48	12.55
J155818.96+241758.7	1851-53524-0476	1.15	11841	17500	7.19	0.89	0.13	8.91
J161047.77+235301.8	1852-53534-0567	—	—	14500	3.40	0.85	0.50	4.57
J074403.80+495439.9	1868-53318-0410	—	—	36390	2.99	0.04	-0.48	50.36
J235503.83+350659.7	1881-53261-0042	—	—	22000	2.84	0.01	0.29	0.18
J235431.39+365019.1	1881-53261-0512	—	—	10500	3.00	0.01	-0.24	73.86
J235318.56+380913.2	1883-53271-0050	1.27	11242	11500	2.39	0.12	-0.32	70.42
J234605.44+385337.6	1883-53271-0272	1.17	24692	14500	45.00	8.92	-0.34	4.71
J235107.47+403453.9	1883-53271-0521	—	—	15000	2.65	0.06	0.20	16.55
J233039.03+500729.6	1889-53240-0377	0.32	11580	14500	1.20	1.26	0.00	33.47
J233708.96+492532.0	1889-53240-0584	0.72	10404	9500	2.08	0.12	-0.28	74.99
J211125.84+110219.6	1890-53237-0390	1.12	15912	11000	2.82	0.35	-0.50	32.99
J224707.31+010058.5	1901-53261-0564	—	—	11000	2.19	0.01	-0.29	75.73
J004148.05-005127.3	1905-53706-0253	—	—	22000	4.39	1.69	0.48	1.40
J014230.56+003502.7	1907-53315-0427	—	—	13000	2.57	0.02	0.36	20.90
J093126.14+321946.1	1943-53386-0294	—	—	18000	12.95	0.06	0.28	0.89
J100657.51+303338.0	1953-53358-0415	0.62	10043	10500	3.23	0.07	-0.50	35.94
J101339.46+352639.6	1954-53357-0250	—	—	21000	2.21	0.91	0.07	5.78
J101428.08+365724.5	1954-53357-0393	0.74	10647	11000	14.93	1.14	-0.36	72.58
J101847.14+304018.0	1956-53437-0143	—	—	30000	3.05	0.04	-0.49	50.98
J101834.81+303330.4	1956-53437-0197	1.15	21262	21000	2.70	0.61	-0.32	72.28
J103935.51+295413.5	1969-53383-0215	1.12	12629	14388	2.40	0.01	0.32	88.17
J113804.15+305310.6	1974-53430-0023	—	—	16500	11.77	0.02	0.28	0.86
J113048.38+305720.6	1974-53430-0222	0.91	10229	10000	3.08	0.01	-0.50	47.33
J112257.10+322327.7	1979-53431-0512	0.98	12687	11500	12.87	0.15	-0.28	50.74
J112014.62+400422.6	1980-53433-0630	1.10	12155	10000	2.54	0.01	-0.36	72.97
J122748.85+385546.3	1986-53475-0090	1.14	16615	13000	8.44	0.28	-0.50	62.18
J125101.98+351913.6	1987-53765-0570	0.87	17874	25000	2.25	1.58	-0.12	0.13
J110203.75+400558.0	1988-53469-0434	0.96	9067	10000	2.11	0.03	0.13	0.01
J125434.64+371000.1	1989-53772-0041	0.74	20196	25365	2.64	5.11	-0.28	0.95
J125709.63+304317.2	1994-53845-0067	0.95	10202	9500	2.44	0.07	-0.30	84.23
J121529.84+335158.6	1999-53503-0238	0.58	16490	25000	2.60	2.20	0.17	0.26
J120924.84+331716.3	2004-53737-0418	0.38	6663	8000	4.03	0.23	-0.26	8.16
J125715.53+341439.3	2006-53476-0332	0.90	9697	9500	22.40	3.91	0.37	89.83

Table 2 continued on next page

Table 2 (continued)

SDSS	Plate-MJD-Fiber	M	T _{eff}	T _{SDSS}	B	$\sigma(B)$	Z _{offset}	incl
		(M _⊙)	(K)	(K)	(MG)	(MG)	(R _*)	(°)
J105152.18+321135.2	2026-53711-0183	1.21	20427	20000	1.30	—	—	33.47
J021148.21+211548.2	2046-53327-0048	1.00	11160	12986	167.11	41.51	-0.31	36.45
J030407.39-002541.9	2048-53378-0280	0.78	12676	9500	10.48	1.37	-0.07	49.81
J080527.55+073534.4	2056-53463-0557	—	—	8000	1.10	0.05	0.00	33.47
J004254.23+235831.5	2058-53349-0087	—	—	10500	2.03	0.01	0.18	10.42
J004038.89+243852.7	2058-53349-0195	—	—	10500	2.52	0.01	-0.36	78.46
J011739.82+242236.2	2060-53706-0086	0.54	11292	10000	2.41	0.04	-0.28	75.24
J012115.44+321010.3	2061-53711-0506	—	—	23000	2.96	0.41	0.02	5.59
J012105.53+393239.7	2062-53381-0337	0.79	25869	21640	2.09	0.00	-0.14	70.73
J012815.71+391130.1	2063-53359-0063	—	—	17000	2.05	0.02	0.11	2.86
J012339.94+405241.9	2063-53359-0403	—	—	50000	4.60	0.04	0.00	33.47
J014313.18+231524.5	2064-53341-0024	—	—	22000	3.00	0.00	0.40	7.55
J013909.14+230844.9	2064-53341-0163	—	—	15500	3.33	0.00	0.45	3.62
J013314.21+235247.4	2064-53341-0343	—	—	40000	9.00	0.10	-0.17	37.96
J013742.53+235138.2	2064-53341-0491	—	—	11500	3.00	0.04	0.37	0.24
J020316.65+220527.2	2066-53349-0302	—	—	11000	2.42	0.01	0.19	0.33
J030647.72+010949.8	2068-53386-0401	—	—	16000	3.08	0.09	0.30	22.83
J040054.81-064625.2	2071-53741-0014	—	—	20000	4.39	0.34	0.18	9.89
J053317.32-004321.9	2072-53430-0096	—	—	40000	16.89	0.58	0.27	7.72
J053016.83-001034.4	2072-53430-0233	—	—	19000	2.34	0.02	0.18	0.32
J052831.02+005244.3	2072-53430-0336	—	—	16444	2.57	0.05	0.24	62.18
J053126.75+001738.1	2072-53430-0427	—	—	13000	2.06	0.02	0.11	15.24
J053507.04+001617.0	2072-53430-0508	—	—	18000	2.42	0.01	0.17	41.67
J073135.36+353108.5	2073-53728-0108	—	—	24000	2.05	0.00	0.03	1.96
J073001.65+362713.2	2073-53728-0482	0.78	16142	10000	2.77	0.02	0.33	84.48
J073237.67+364628.8	2073-53728-0571	1.34	27417	20000	108.72	28.00	-0.03	69.82
J074047.65+180907.3	2074-53437-0237	0.77	22775	23000	1.70	0.36	0.00	33.47
J074327.09+273732.4	2075-53730-0278	—	—	9500	2.28	0.05	-0.31	69.75
J080905.97+062441.7	2076-53442-0076	0.18	9903	18000	2.25	0.09	0.18	87.64
J080638.50+075647.5	2076-53442-0521	—	—	21000	2.11	0.69	-0.26	56.26
J073953.17+204900.2	2079-53379-0051	—	—	22000	2.01	0.03	0.11	15.63
J074958.58+161120.2	2080-53350-0349	—	—	24000	2.09	0.00	0.03	5.77
J080440.35+182730.9	2081-53357-0442	0.89	9749	10135	38.26	25.56	-0.12	16.04
J081716.39+200834.9	2082-53358-0444	0.74	6901	8000	3.78	0.21	-0.28	9.66
J082107.34+194433.6	2082-53358-0617	—	—	25000	1.30	—	—	33.47
J083041.77+204233.7	2083-53359-0553	1.00	18687	17500	2.19	0.06	-0.19	77.75
J083918.12+212143.7	2084-53360-0100	1.05	12139	13500	3.40	—	—	33.47
J084936.81+224754.9	2085-53379-0131	1.08	29177	25000	2.10	0.49	0.12	9.03
J090937.94+250820.6	2086-53401-0582	0.86	10024	10500	2.52	0.10	-0.39	50.91
J091305.58+260748.5	2087-53415-0383	—	—	16000	2.30	0.00	0.18	19.84

Table 2 continued on next page

Table 2 (continued)

SDSS	Plate-MJD-Fiber	M	T _{eff}	T _{SDSS}	B	$\sigma(B)$	Z _{offset}	incl
		(M _⊙)	(K)	(K)	(MG)	(MG)	(R _*)	(°)
J120547.47+340811.4	2089-53498-0431	0.74	18605	17500	9.74	0.07	-0.35	60.80
J105833.57+372401.3	2091-53447-0464	0.90	11395	9500	2.55	0.04	0.19	84.90
J115817.44+331719.2	2095-53474-0337	—	—	24000	2.03	0.00	0.11	4.10
J140051.72+330754.3	2121-54180-0369	0.56	23055	30000	3.15	1.04	0.28	5.69
J141813.21+312340.0	2129-54252-0426	0.68	7457	8000	2.55	0.12	-0.37	17.57
J141906.19+254356.4	2131-53819-0317	0.83	9205	9500	2.27	0.30	-0.30	60.26
J143019.05+281100.8	2134-53876-0423	0.94	9052	9000	7.26	1.09	-0.15	18.21
J151606.34+274647.0	2154-54539-0637	0.87	67365	30000	3.03	0.06	-0.44	75.43
J152203.44+203438.9	2156-54525-0031	0.45	17315	14000	2.98	0.03	0.26	0.85
J154856.93+230727.9	2169-53556-0491	—	—	9732	2.81	0.10	-0.42	62.80
J163600.24+354625.3	2185-53532-0320	0.46	17391	25000	9.97	3.71	0.48	3.71
J161344.78+174609.0	2188-54595-0406	0.29	13175	15500	2.96	0.09	0.43	32.14
J165651.45+243802.7	2191-54621-0608	0.26	11866	10500	2.54	0.00	-0.34	69.36
J165439.46+391103.3	2192-54232-0310	0.66	8296	9500	2.43	0.01	-0.24	60.16
J172735.80+280536.8	2193-53888-0570	0.45	18057	18084	2.14	0.06	0.22	87.87
J174755.71+251232.3	2194-53904-0154	0.67	10993	10500	2.29	0.03	-0.30	84.15
J161321.40+155332.0	2198-53918-0400	0.57	10983	9500	3.30	0.02	0.47	4.03
J161147.94+211136.6	2205-53793-0542	0.66	11382	10000	2.19	0.00	0.23	5.58
J163400.34+145651.3	2209-53907-0472	—	—	15500	5.50	0.00	0.25	8.55
J112439.29+262422.7	2216-53795-0143	1.03	21151	10500	2.33	0.01	0.32	79.21
J113055.04+260115.6	2218-53816-0081	—	—	24000	2.40	0.01	0.00	33.47
J113215.38+280934.3	2219-53816-0329	—	—	8000	2.77	0.16	-0.33	9.00
J113500.52+291206.5	2220-53795-0222	—	—	25000	2.02	0.01	0.03	2.30
J114529.26+300824.3	2222-53799-0483	0.54	14836	15000	3.33	0.02	0.49	5.41
J114833.24+303921.2	2222-53799-0577	0.49	9411	18000	2.65	0.24	0.32	42.73
J114917.22+300016.0	2222-53799-0593	0.30	9344	9000	2.75	0.08	-0.37	65.19
J130535.77+283014.5	2242-54153-0447	—	—	24000	2.42	0.01	0.17	29.06
J131544.04+262333.3	2243-53794-0170	0.85	8872	12000	3.56	0.00	0.48	3.15
J131702.34+281848.6	2243-53794-0533	0.40	11819	9500	2.27	0.01	-0.21	64.31
J132926.04+254936.4	2245-54208-0307	1.37	28492	28299	2.61	0.18	-0.39	54.04
J202501.10+131025.6	2257-53612-0167	0.56	13790	28932	10.06	0.69	0.15	10.28
J203256.47+142652.1	2258-54328-0278	—	—	24000	3.50	1.73	0.38	49.60
J203332.93+140115.4	2258-54328-0295	—	—	18529	2.16	0.01	-0.15	87.96
J205000.93+170145.5	2259-53565-0530	—	—	22000	3.11	0.70	0.06	8.12
J224829.60+223355.9	2261-53612-0075	—	—	10000	37.11	3.43	-0.32	0.64
J224602.81+230704.1	2261-53612-0559	0.77	17130	15500	2.06	0.06	0.18	0.34
J080359.93+122943.9	2265-53674-0033	—	—	12347	33.29	4.86	-0.35	16.97
J075816.63+121428.6	2265-53674-0199	0.79	13521	10000	2.50	0.03	-0.35	71.82
J080210.39+153033.8	2266-53679-0534	0.99	17869	19000	2.01	0.01	0.11	19.88
J080703.25+135537.8	2268-53682-0472	0.54	11082	20000	2.81	0.25	0.02	3.97

Table 2 continued on next page

Table 2 (continued)

SDSS	Plate-MJD-Fiber	M	T _{eff}	T _{SDSS}	B	$\sigma(B)$	Z _{offset}	incl
		(M _⊙)	(K)	(K)	(MG)	(MG)	(R _*)	(°)
J081748.55+154341.1	2272-53713-0386	0.52	12054	11000	1.80	—	—	33.47
J082817.60+181752.6	2275-53709-0298	0.77	20127	13000	2.19	0.01	0.13	31.43
J083613.81+201852.1	2275-53709-0526	—	—	9500	2.96	0.02	-0.33	71.70
J083701.89+154454.6	2276-53712-0004	0.97	21399	17000	3.00	0.01	0.43	8.66
J083627.34+154850.3	2276-53712-0107	1.09	36312	30000	5.03	4.59	0.5	3.75
J083623.85+163859.6	2278-53711-0270	1.10	13998	11000	2.58	0.11	-0.38	53.83
J085129.15+195205.4	2280-53680-0018	0.85	8724	9500	3.00	0.02	-0.42	75.49
J084845.65+214047.0	2280-53680-0446	0.62	20534	24000	3.43	1.14	0.37	17.55
J090522.06+205736.2	2284-53708-0091	0.43	10902	19000	2.21	0.73	0.13	52.90
J090554.63+213829.5	2284-53708-0103	0.33	18045	30000	2.10	0.06	0.00	33.47
J090907.15+193840.6	2286-53700-0176	—	—	14000	2.99	0.01	0.43	27.95
J091132.79+223200.6	2287-53705-0169	0.76	11884	11500	3.07	0.01	0.40	0.40
J091002.83+232219.9	2287-53705-0470	—	—	21000	2.28	0.56	-0.03	18.84
J091310.43+230042.6	2287-53705-0541	—	—	23000	2.10	1.20	0.08	4.79
J091326.64+211250.4	2288-53699-0332	0.61	13537	15500	2.23	0.01	0.26	84.06
J091526.57+205039.1	2288-53699-0468	—	—	11000	2.05	0.02	0.11	33.14
J093059.15+202429.3	2289-53708-0069	0.61	10459	15000	3.19	0.39	0.43	16.14
J092355.96+243552.8	2291-53714-0552	—	—	17000	5.34	0.24	0.25	30.87
J094025.97+201707.2	2292-53713-0048	—	—	10500	2.00	0.01	0.00	33.47
J093654.94+262650.2	2294-54524-0617	—	—	23000	3.73	1.87	0.38	9.85
J055814.96+643826.5	2301-53712-0344	—	—	12000	3.00	0.00	0.44	8.97
J060442.48+641357.1	2301-53712-0476	0.78	21586	13000	20.75	0.89	-0.44	18.59
J053400.83+625419.7	2302-53709-0579	—	—	8000	2.19	0.02	0.13	62.91
J225726.05+075541.6	2310-53710-0420	—	—	9500	17.40	9.54	-0.44	40.16
J091833.32+205536.9	2319-53763-0209	—	—	15584	2.55	0.42	-0.28	75.50
J091629.56+215011.4	2319-53763-0236	0.69	5883	8000	6.19	0.20	-0.15	24.48
J092041.53+221545.4	2319-53763-0557	—	—	24000	2.09	0.01	-0.10	49.93
J092246.94+230812.6	2319-53763-0567	—	—	21000	2.61	0.02	0.20	57.24
J212329.46-081004.4	2320-54653-0090	—	—	15500	2.29	0.52	0.13	18.30
J211744.74-073652.8	2320-54653-0312	—	—	32642	2.48	0.03	-0.40	26.25
J212143.07-060005.7	2320-54653-0445	0.77	17082	25075	1.94	0.03	-0.10	53.26
J212232.58-061839.6	2320-54653-0537	—	—	10500	3.00	0.03	0.41	0.86
J212425.74-064837.2	2320-54653-0544	0.77	9638	16822	2.30	0.01	0.29	89.23
J212514.18-062152.5	2320-54653-0612	—	—	17000	2.10	1.39	0.15	4.36
J021338.51+053023.3	2321-53711-0125	—	—	8500	2.42	0.02	-0.29	67.74
J021107.71+072235.4	2321-53711-0409	—	—	14000	2.19	0.01	0.28	28.13
J030522.15+050213.3	2322-53727-0024	0.49	8987	13500	2.95	0.67	0.43	9.01
J030107.56+053956.9	2322-53727-0136	—	—	18000	2.29	0.05	-0.17	58.18
J004011.48+070255.6	2327-53710-0074	0.82	12408	12000	3.12	0.06	0.42	8.42
J003223.65+082329.5	2327-53710-0321	0.69	9072	11000	2.19	0.01	-0.31	47.14

Table 2 continued on next page

Table 2 (continued)

SDSS	Plate-MJD-Fiber	M	T _{eff}	T _{SDSS}	B	$\sigma(B)$	Z _{offset}	incl
		(M _⊙)	(K)	(K)	(MG)	(MG)	(R _*)	(°)
J012215.76+082712.7	2329-53725-0370	—	—	8000	2.57	0.02	-0.36	82.14
J083310.56+234812.7	2330-53738-0109	—	—	10500	3.00	0.00	0.44	17.77
J083051.08+244615.7	2330-53738-0503	—	—	11000	2.29	0.01	-0.31	81.05
J083531.17+533230.8	2331-53742-0197	0.78	8379	8000	14.40	4.25	-0.46	10.46
J032658.77+040307.9	2339-53729-0046	1.32	27169	13000	2.82	0.21	-0.42	68.94
J032628.17+052136.2	2339-53729-0515	0.92	21233	16000	15.95	0.52	-0.49	20.38
J031058.73+045129.9	2340-53733-0165	0.51	9918	9000	2.55	0.03	-0.27	80.11
J100426.98+223810.5	2343-53735-0300	—	—	10500	2.29	0.01	0.29	75.82
J101642.26+281610.2	2348-53757-0040	0.91	25367	25000	2.16	0.00	0.07	6.60
J100727.32+281457.8	2348-53757-0279	—	—	11500	2.07	0.00	0.12	29.33
J101059.21+284359.6	2348-53757-0485	—	—	19000	2.00	—	—	33.47
J102220.69+272539.8	2350-53765-0543	1.20	16227	17000	8.23	0.93	0.42	17.63
J102535.39+282034.8	2351-53772-0007	—	—	24000	2.38	0.01	-0.12	10.24
J102429.16+281435.4	2351-53786-0001	0.31	11778	21000	2.20	0.81	-0.22	59.98
J103403.98+305034.4	2354-53799-0536	0.74	15302	12500	2.77	0.02	0.27	1.27
J104851.93+273817.6	2358-53797-0156	—	—	9000	2.03	0.02	0.14	28.23
J092524.25+175712.6	2360-53728-0217	0.53	12343	17314	2.00	0.01	-0.26	81.68
J093726.27+205756.9	2361-53762-0408	1.05	12875	18000	5.44	0.01	0.13	58.49
J095738.55+194601.8	2363-53763-0097	—	—	18000	2.09	0.00	0.14	8.03
J100828.97+183633.4	2373-53768-0290	0.71	10047	13000	2.38	0.00	0.17	2.09
J102239.05+194904.2	2374-53765-0544	0.89	9002	9000	3.23	0.16	-0.50	47.12
J103350.87+204729.3	2376-53770-0463	1.12	15958	16500	10.91	0.15	-0.49	27.32
J103532.53+212603.5	2376-53770-0534	—	—	8000	2.77	0.15	-0.35	18.17
J024903.01+332737.0	2398-53768-0313	0.26	11136	9500	2.66	0.02	-0.26	85.98
J023542.72+241653.7	2399-53764-0030	—	—	9500	2.33	0.00	0.17	85.49
J023449.24+240750.2	2399-53764-0070	0.55	5419	8000	3.59	0.16	-0.29	15.23
J023035.63+250831.5	2399-53764-0164	0.55	5662	8000	4.19	0.17	-0.25	16.87
J023157.00+264837.5	2399-53764-0426	1.10	11056	9500	2.29	1.57	-0.19	70.17
J023445.31+260553.1	2399-53764-0487	—	—	13000	6.65	1.37	0.04	5.79
J023420.62+264801.6	2399-53764-0559	0.82	13560	40000	30.78	3.45	-0.02	13.13
J085403.30+361121.3	2400-53765-0291	0.62	9880	10500	2.57	0.17	-0.35	82.77
J093813.82+615600.8	2403-53795-0278	1.07	19840	10500	2.49	0.01	0.22	8.34
J094210.10+521313.3	2404-53764-0058	0.56	8045	8000	2.57	0.14	-0.39	49.68
J105732.05+480125.9	2410-54087-0117	1.01	11795	16000	2.29	0.01	-0.32	88.98
J105556.92+483652.4	2410-54087-0494	—	—	9500	2.19	0.00	-0.28	66.87
J111608.80+092532.5	2413-54169-0151	0.55	5212	8000	1.40	0.06	-0.19	17.69
J110911.12+582209.3	2414-54526-0301	—	—	30000	2.95	1.02	0.23	37.43
J111010.50+600141.3	2414-54526-0323	1.23	32216	19500	8.12	0.02	-0.5	50.70
J031929.01+410316.9	2417-53766-0064	—	—	10000	3.15	0.00	0.46	1.01
J031824.19+422651.0	2417-53766-0568	0.89	11285	8500	8.48	0.99	0.03	44.11

Table 2 continued on next page

Table 2 (continued)

SDSS	Plate-MJD-Fiber	M	T _{eff}	T _{SDSS}	B	$\sigma(B)$	Z _{offset}	incl
		(M _⊙)	(K)	(K)	(MG)	(MG)	(R _*)	(°)
J082447.49+131543.2	2422-54096-0588	—	—	22000	1.70	0.23	0.00	33.47
J083420.29+131759.5	2426-53795-0387	—	—	21000	4.50	0.01	0.11	2.73
J083438.28+153817.5	2427-53815-0321	—	—	16500	5.59	0.00	0.28	0.08
J084510.22+112405.6	2428-53801-0089	0.43	9132	16000	2.17	0.08	0.15	12.40
J084219.70+122128.3	2428-53801-0221	—	—	20000	2.04	0.66	0.12	13.71
J084039.36+125706.2	2428-53801-0354	0.40	9487	12000	2.22	0.01	0.17	0.37
J084522.94+150020.3	2429-53799-0152	—	—	18000	2.03	0.02	0.17	22.64
J084111.34+154921.0	2429-53799-0358	—	—	19000	2.65	0.00	0.25	43.13
J084201.41+153941.8	2429-53799-0363	0.60	16480	20000	18.12	0.01	0.25	81.62
J085106.12+120157.8	2430-53815-0229	0.90	11246	10000	2.28	0.43	-0.30	68.87
J085153.78+152724.9	2431-53818-0238	0.85	12056	10000	26.97	9.86	-0.15	65.59
J091305.88+173932.9	2439-53795-0357	—	—	17500	2.76	0.15	0.36	0.18
J030913.96+373057.9	2443-54082-0030	—	—	19000	2.30	0.02	0.00	33.47
J030432.88+365537.8	2443-54082-0137	—	—	18500	2.20	0.01	-0.04	13.32
J030550.34+370759.1	2443-54082-0154	0.48	10492	10500	3.00	0.02	0.36	0.04
J030158.92+372204.2	2443-54082-0190	—	—	12500	3.00	0.09	0.40	14.86
J024241.66+291608.2	2444-54082-0604	0.37	10135	12000	3.36	0.05	0.50	10.53
J024505.94+282542.7	2444-54082-0623	0.75	5699	8000	1.40	0.05	-0.15	7.55
J124836.31+294231.2	2457-54180-0112	0.61	6853	8000	2.19	0.11	-0.39	5.36
J133836.06+652433.1	2460-54616-0042	—	—	19000	2.19	0.01	0.16	0.63
J130033.46+590406.9	2461-54570-0015	0.57	6123	8000	6.72	0.27	-0.12	36.05
J125040.81+590341.6	2461-54570-0219	0.78	15740	30000	2.80	0.01	0.00	33.47
J124508.48+591551.6	2461-54570-0264	0.38	19065	24000	1.10	—	—	33.47
J141710.80+573546.1	2462-54561-0404	0.74	5585	8000	2.50	0.07	-0.04	23.52
J155232.76+264636.6	2474-54564-0392	0.75	20123	19362	1.10	—	—	33.47
J154550.71+132040.2	2517-54567-0065	0.50	12940	10000	2.81	0.02	-0.32	77.09
J154424.84+132650.8	2517-54567-0110	0.68	11289	13000	2.06	0.07	0.22	27.14
J160357.92+140929.9	2524-54568-0247	0.82	8860	9500	49.40	58.55	-0.24	52.38
J160219.42+112606.4	2525-54569-0303	0.99	10337	9500	2.53	0.00	-0.03	37.90
J160532.18+131748.6	2525-54569-0425	—	—	19000	1.70	0.08	0.00	33.47
J161050.03+094302.4	2526-54582-0115	—	—	25000	2.70	—	—	33.47
J160540.06+093724.8	2526-54582-0223	0.58	25128	16000	2.17	0.01	0.17	19.33
J161929.62+131833.4	2530-53881-0332	0.63	20084	22000	2.90	—	—	33.47
J163013.93+123941.9	2533-54585-0325	0.33	10720	13500	2.08	0.01	0.17	0.30
J163630.30+114452.2	2533-54585-0502	0.69	10189	10500	3.00	0.00	0.42	2.18
J064828.77+840340.8	2548-54152-0616	1.07	13038	11500	3.73	0.01	-0.17	53.66
J085550.69+824905.2	2549-54523-0066	1.14	21375	32081	12.19	0.15	0.23	66.09
J083448.65+821059.0	2549-54523-0135	1.17	24915	23000	15.02	0.92	-0.39	55.53
J174235.20+640028.3	2561-54597-0021	—	—	30000	2.00	0.01	0.00	33.47
J173208.55+631950.3	2561-54597-0087	—	—	24000	2.30	0.02	-0.14	6.73

Table 2 continued on next page

Table 2 (continued)

SDSS	Plate-MJD-Fiber	M	T _{eff}	T _{SDSS}	B	$\sigma(B)$	Z _{offset}	incl
		(M _⊙)	(K)	(K)	(MG)	(MG)	(R _*)	(°)
J172623.13+632607.8	2561-54597-0212	—	—	25000	2.85	0.02	0.07	87.22
J192553.59+620708.6	2563-54653-0165	0.90	10093	9000	2.28	0.01	-0.31	86.27
J192416.73+614833.1	2563-54653-0255	—	—	9500	2.58	0.01	-0.38	54.85
J102746.58+435156.2	2567-54179-0306	0.25	9266	9500	2.11	0.03	-0.15	74.41
J121840.75-001005.8	2568-54153-0309	—	—	25000	2.33	0.00	0.16	89.99
J122238.86+005034.4	2568-54153-0411	0.24	10410	13500	2.19	0.01	0.15	10.81
J122209.43+001534.1	2568-54153-0471	—	—	19500	8.00	0.02	0.27	0.79
J081523.35+084346.4	2571-54055-0256	—	—	21000	5.17	0.02	0.17	0.41
J082939.24+100937.7	2572-54056-0399	0.99	15640	22000	2.69	0.71	-0.21	81.09
J084011.39+094244.8	2573-54061-0130	0.42	7931	9500	2.19	0.01	0.20	5.30
J084233.36+101806.3	2573-54061-0141	—	—	12284	2.78	0.01	0.35	77.36
J083801.80+092548.3	2573-54061-0246	—	—	23000	3.77	0.13	0.44	1.37
J091340.18+114112.3	2576-54086-0029	0.64	11484	17500	2.19	0.04	0.18	11.19
J091611.06+124808.0	2577-54086-0427	0.78	23461	22000	2.12	0.41	-0.10	8.54
J092108.83+130111.6	2577-54086-0448	0.65	10326	20000	2.47	0.98	0.01	0.40
J093431.10+132814.6	2580-54092-0273	—	—	34332	2.13	0.02	-0.24	62.35
J100758.24+163618.9	2585-54097-0024	—	—	11000	2.27	0.05	-0.31	79.19
J100759.80+162349.6	2585-54097-0030	1.01	10671	32642	13.02	9.31	-0.12	40.83
J100645.00+144250.3	2586-54169-0479	—	—	12000	2.78	0.01	0.40	10.44
J102230.51+144646.8	2590-54175-0191	0.98	7664	8500	2.22	0.03	0.15	1.04
J103002.66+163927.4	2592-54178-0417	—	—	22000	4.01	0.00	0.18	0.47
J103648.66+171045.1	2593-54175-0131	0.42	12309	9500	2.19	0.01	-0.13	78.82
J121706.46+172855.9	2596-54207-0023	0.41	28189	25000	1.20	—	—	33.47
J125511.49+154929.7	2602-54149-0249	0.44	13804	10000	2.24	0.01	-0.30	72.69
J131426.37+173228.0	2604-54484-0481	0.79	7022	8000	2.62	0.15	-0.35	13.68
J121211.27+185228.9	2609-54476-0005	—	—	25000	10.92	1.22	0.50	3.81
J121110.29+203429.0	2609-54476-0564	—	—	25000	2.26	0.01	0.11	0.15
J132203.94+193223.1	2619-54506-0423	—	—	18000	4.09	1.27	0.17	1.92
J225123.66+293945.3	2621-54380-0042	—	—	8000	1.80	0.08	-0.17	29.36
J225338.68+301803.4	2627-54379-0021	1.10	19805	23000	2.01	0.01	0.14	12.68
J224854.51+303845.5	2627-54379-0152	—	—	22000	4.05	1.93	0.49	3.58
J121033.23+221402.6	2644-54210-0167	0.91	13414	10500	2.23	1.65	-0.30	59.99
J133025.70+224813.6	2653-54230-0408	0.67	12660	10000	3.19	0.01	-0.48	61.25
J122100.20+244443.7	2657-54502-0026	0.47	9549	10500	2.25	0.01	-0.30	59.35
J044254.59+120329.8	2669-54086-0377	0.76	9349	8000	33.72	14.03	-0.34	56.07
J044641.49+101510.9	2673-54096-0049	0.75	9567	8000	2.17	0.16	-0.29	57.95
J082108.17+372738.3	2674-54097-0103	—	—	8000	0.60	0.00	-0.33	16.25
J034630.98+094827.4	2679-54368-0225	1.28	26236	19500	2.79	0.33	0.32	89.23
J034314.34+102938.3	2679-54368-0356	1.03	42617	40000	8.57	4.02	-0.50	37.73
J064607.86+280510.0	2694-54199-0175	—	—	19500	2.28	0.06	-0.31	65.18

Table 2 continued on next page

Table 2 (*continued*)

SDSS	Plate-MJD-Fiber	M	T _{eff}	T _{SDSS}	B	$\sigma(B)$	Z _{offset}	incl
		(M _⊙)	(K)	(K)	(MG)	(MG)	(R _*)	(°)
J064532.74+280330.4	2694-54199-0201	0.46	10522	11351	2.30	—	—	33.47
J065133.33+284423.3	2694-54199-0528	—	—	17841	2.16	0.09	0.15	8.36
J071814.18+305148.8	2695-54409-0268	—	—	12000	3.19	3.33	0.47	5.48
J072540.81+321402.1	2695-54409-0564	—	—	24000	15.15	0.88	0.29	57.89
J035010.32+085829.1	2697-54389-0048	—	—	14500	2.02	0.01	0.16	0.27
J072724.65+403622.4	2701-54154-0301	1.13	13501	10500	2.81	0.13	-0.37	72.98
J075234.95+172524.9	2729-54419-0171	0.80	8665	9000	12.68	1.17	-0.31	48.59
J074924.91+171355.3	2729-54419-0282	0.68	20941	18500	14.95	0.41	-0.39	57.16
J140709.72+154010.2	2745-54231-0343	0.84	11486	13500	22.82	0.00	-0.12	62.17
J152936.81+123436.8	2754-54240-0371	0.36	12209	10500	2.52	0.07	-0.36	73.12
J151436.65+152058.4	2766-54242-0497	0.94	9386	10500	3.08	0.15	-0.49	50.42
J140444.21+201922.6	2771-54527-0196	0.66	17354	14500	2.13	0.01	-0.24	76.47
J141309.30+191831.9	2772-54529-0217	1.19	16400	14000	2.53	0.05	-0.31	67.01
J154141.84+173026.2	2795-54563-0603	1.01	15425	16500	2.19	0.00	0.15	0.51
J164649.56+120547.0	2817-54627-0308	0.77	30172	40000	3.07	0.08	-0.47	54.72
J165413.92+124344.7	2817-54627-0553	0.56	5287	8000	1.45	0.05	-0.17	13.46
J172704.99+084857.1	2818-54616-0374	0.54	33635	40000	1.10	0.07	0.00	33.47
J184130.70+410745.1	2819-54617-0104	0.63	5902	8000	1.40	0.09	-0.13	4.28
J173056.41+433000.4	2820-54599-0185	—	—	20000	2.45	0.65	-0.04	0.93
J001034.94+245131.2	2822-54389-0025	0.98	9064	10500	11.80	0.30	-0.32	57.32
J000701.59+240744.8	2822-54389-0042	—	—	8000	2.27	0.01	-0.30	64.61
J011130.67+141049.7	2825-54439-0089	—	—	19000	3.30	0.84	0.32	2.27
J080620.12-075457.1	2827-54422-0307	1.32	10446	9000	3.19	0.01	0.30	28.06
J083234.10-042813.7	2828-54438-0149	—	—	9500	7.90	0.00	0.35	5.97
J020514.52+003100.3	2866-54478-0603	—	—	18000	2.42	0.03	0.22	3.50
J111245.75+185719.5	2872-54533-0233	—	—	8500	2.52	0.17	-0.36	56.52
J111205.21+183200.2	2872-54533-0284	—	—	9000	2.57	0.06	-0.39	40.01
J112216.02-122250.9	2874-54561-0071	—	—	13500	3.15	0.02	0.46	1.16
J111539.09-111350.6	2874-54561-0333	0.46	5543	8000	4.64	0.22	-0.22	2.66
J112030.34-115051.1	2874-54561-0512	1.30	28653	15500	9.59	0.02	-0.49	44.33
J012516.68-101313.7	2878-54465-0269	—	—	11500	2.61	0.02	0.25	0.04
J161425.46+493244.9	2884-54526-0254	0.32	11384	11500	3.00	0.01	0.44	7.93
J093415.96+294500.4	2914-54533-0162	0.69	17852	40000	32.01	0.74	0.35	42.92
J075036.54+222021.4	2916-54507-0133	—	—	21000	2.08	0.00	0.08	33.22
J123706.24-001603.9	2920-54562-0110	1.01	10947	11000	2.55	0.01	-0.38	62.18
J124851.30-022924.7	2922-54612-0607	0.74	13658	9500	4.26	0.40	-0.15	16.53
J135206.28+175333.0	2930-54589-0051	—	—	8000	2.19	0.02	0.16	11.14
J143235.46+454852.4	2932-54595-0542	0.73	15821	22000	11.72	1.93	0.43	9.51
J044512.39-052524.5	2942-54521-0487	—	—	18000	2.68	0.28	0.24	5.82
J045016.37-053847.8	2942-54521-0637	—	—	40000	2.15	0.01	0.16	2.94

Table 2 *continued on next page*

Table 2 (continued)

SDSS	Plate-MJD-Fiber	M	T _{eff}	T _{SDSS}	B	$\sigma(B)$	Z _{offset}	incl
		(M _⊙)	(K)	(K)	(MG)	(MG)	(R _*)	(°)
J071410.25+401219.4	2943-54502-0612	—	—	18000	2.35	0.01	0.15	88.78
J075137.54+670732.3	2944-54523-0569	0.65	5440	8000	0.90	0.00	-0.17	12.87
J075704.00+085519.9	2945-54505-0148	—	—	22000	1.60	0.14	0.00	33.47
J153349.02+005916.1	2954-54561-0048	0.61	12327	9500	2.62	0.48	-0.17	65.27
J154524.79+010127.5	2955-54562-0061	—	—	19500	2.40	0.03	0.00	33.47
J084541.11+312936.6	2960-54561-0009	—	—	12500	2.08	0.33	0.18	0.45
J160904.12+175337.7	2967-54584-0089	0.57	11595	9000	2.43	0.17	-0.24	72.96
J031637.81-003310.9	3183-54833-0179	0.59	7011	9000	2.00	0.17	-0.30	9.35
J071632.91+393553.8	3655-55240-0488	0.65	14947	17000	2.44	0.30	0.22	87.60
J073615.91+403335.0	3658-55205-0062	0.81	6488	8000	3.79	0.19	-0.27	14.46
J073741.49+470421.1	3665-55247-0394	0.40	25490	23000	3.59	0.66	0.49	3.55
J074126.28+394118.7	3670-55480-0528	0.66	6611	8000	1.45	0.03	-0.24	9.23
J075916.53+433518.9	3676-55186-0030	1.37	20912	22420	2.29	0.00	-0.27	44.98
J081632.25+522645.2	3689-55180-0826	0.60	7235	8000	2.19	0.36	-0.40	0.39
J083051.14+503610.7	3694-55209-0966	0.96	18201	16000	2.26	0.15	0.30	72.81
J093054.58-012642.9	3767-55214-0562	1.15	13898	10500	10.42	1.05	-0.32	7.09
J113839.49-014903.0	3775-55207-0698	0.76	11717	9500	24.33	5.06	-0.15	62.90
J084906.22+003722.8	3813-55532-0364	0.77	14065	14500	18.27	4.40	-0.45	64.16
J090855.40+010552.5	3818-55532-0906	0.62	7744	8000	3.00	0.02	-0.33	48.63
J094416.62-001855.5	3827-55565-0472	0.55	7926	8000	3.77	0.02	-0.28	17.50
J112059.67-001942.2	3838-55588-0064	0.92	30253	19000	3.26	0.16	0.47	4.22
J134820.79+381017.2	3852-55243-0676	1.29	30979	25000	15.52	4.67	-0.36	59.10
J134024.99+325028.7	3856-55269-0462	0.69	27311	25000	2.36	0.31	-0.07	59.41
J151835.81+311911.4	3879-55244-0584	—	—	8500	2.61	0.08	-0.23	71.71
J155202.55+170434.7	3926-55327-0738	0.86	7436	8000	2.62	0.02	-0.36	16.89
J152401.59+185659.2	3945-55648-0726	1.06	13793	9500	6.49	0.97	-0.18	21.15
J154855.04+245112.9	3947-55332-0016	1.20	21234	17500	8.41	1.30	-0.39	69.19
J151516.47+244547.7	3961-55654-0708	0.92	9113	8000	16.39	1.88	-0.46	67.54
J150809.79+215037.0	3962-55660-0428	0.61	16595	15000	17.50	2.77	-0.47	27.66
J131955.04+015259.5	4006-55328-0358	0.31	13501	12500	3.24	0.09	0.48	5.30
J145231.59-025634.1	4023-55328-0122	0.77	11993	11500	2.28	0.28	-0.32	72.23
J143147.14+012153.0	4024-55646-0304	0.57	15667	12000	2.72	0.14	0.39	74.35
J162304.10+183522.2	4060-55359-0296	0.50	12044	14000	2.50	0.07	0.28	81.41
J163334.67+194229.7	4061-55362-0761	0.64	15308	17500	2.67	0.50	-0.38	44.55
J163350.80+150822.6	4068-55445-0746	—	—	40000	3.52	12.01	0.50	3.81
J162216.01+184019.4	4073-55663-0806	0.74	20596	16500	3.43	0.08	0.50	6.56
J163917.45+103604.9	4075-55352-0101	0.72	6300	8000	1.45	0.06	-0.21	16.94
J211504.83+040009.7	4077-55361-0564	0.59	6321	8000	4.50	0.31	-0.23	5.82
J213148.69+065930.1	4085-55452-0074	0.88	7535	8000	31.14	9.18	-0.25	9.37
J214536.12+062726.8	4091-55498-0588	0.59	19353	17000	2.07	0.21	0.27	79.52

Table 2 continued on next page

Table 2 (continued)

SDSS	Plate-MJD-Fiber	M	T _{eff}	T _{SDSS}	B	$\sigma(B)$	Z _{offset}	incl
		(M _⊙)	(K)	(K)	(MG)	(MG)	(R _*)	(°)
J162808.39+233254.1	4184-55450-0844	—	—	8000	4.77	0.21	-0.09	32.98
J164359.14+273047.7	4190-55686-0984	0.62	18269	10500	2.86	0.04	0.27	51.96
J004528.87+004616.4	4223-55451-0634	1.29	22391	19500	2.19	0.08	-0.26	61.77
J021116.37+003128.2	4235-55451-0850	0.85	9183	9000	31.06	8.84	-0.24	8.18
J021818.18+035525.3	4264-55506-0408	0.94	7982	8000	2.46	0.01	-0.36	20.28
J231951.71+010908.7	4286-55499-0125	—	—	30000	2.40	0.20	-0.36	68.91
J020002.57-020542.3	4349-55803-0892	0.75	7104	8000	2.77	0.32	-0.33	38.09
J082302.39+334534.1	4442-55532-0578	0.87	7752	8000	2.46	0.08	-0.37	8.84
J074213.39+315703.8	4443-55539-0256	0.75	9562	9000	41.40	25.36	-0.16	11.24
J083446.91+304959.2	4449-55544-0876	0.47	21780	11500	2.56	0.1	-0.36	85.31
J081819.51+225349.9	4468-55894-0368	—	—	35245	2.54	0.21	0.36	89.04
J081354.17+223713.6	4469-55863-0047	0.89	22106	21000	15.52	2.46	0.36	77.38
J074224.66+232804.1	4470-55587-0200	0.99	12378	14000	2.84	0.28	-0.35	55.65
J083945.55+200015.7	4484-55565-0072	0.73	14964	15500	2.72	0.26	-0.27	59.18
J083020.35+185814.5	4489-55545-0678	1.13	21250	20000	2.27	0.01	-0.30	80.38
J074907.48+154534.1	4495-55566-0435	0.54	19493	22000	2.09	0.08	-0.25	73.24
J080359.93+122943.9	4505-55603-0384	1.13	17756	17500	34.76	8.70	-0.33	30.89
J081216.23+131708.2	4505-55603-0987	0.45	13565	18000	2.66	0.24	0.23	4.15
J000603.80+075514.4	4534-55863-0248	0.76	9102	9000	12.94	9.04	-0.47	43.92
J102054.10+362647.0	4568-55600-0952	0.71	15917	13500	61.20	12.02	-0.20	52.99
J091124.68+420255.8	4603-55999-0200	0.87	9761	10500	44.50	8.59	-0.11	53.70
J113114.44+355007.2	4618-55600-0022	0.61	15023	12500	3.00	0.16	0.43	1.85
J094111.40+423921.2	4638-55956-0034	—	—	40000	3.48	0.02	0.49	59.24
J101507.34+441507.8	4693-55632-0066	—	—	8000	2.77	0.08	-0.33	20.30
J124816.81+411051.2	4703-55617-0381	0.68	20586	13500	3.09	0.11	-0.50	50.82
J142703.35+372110.5	4713-56044-0230	1.16	18983	14500	32.06	6.16	-0.35	65.56
J142836.95+383904.9	4713-56044-0844	0.66	7537	8000	7.00	0.55	-0.36	10.53
J154012.07+290828.9	4722-55735-0206	0.25	19833	40000	11.95	0.30	-0.49	17.53
J103724.11+013528.8	4734-55646-0298	1.17	14893	10500	3.73	2.38	-0.50	14.07
J092926.44+013535.6	4742-55660-0420	0.94	16856	13000	2.26	0.08	-0.29	79.55
J130805.95+035424.3	4760-55656-0470	0.60	20585	13000	2.19	0.13	0.30	73.67
J103430.15+032736.3	4772-55654-0128	1.10	15747	11500	13.28	1.87	-0.28	65.82
J150451.71+052141.0	4776-55652-0509	1.13	16080	17500	5.25	0.18	-0.32	69.96
J133420.95+041751.3	4786-55651-0518	1.17	15097	17415	2.43	0.15	-0.27	73.80
J081656.46+030417.0	4787-55863-0846	0.61	6879	8000	4.19	0.33	-0.25	15.71
J100356.31+053825.6	4800-55674-0790	—	—	22000	163.51	18.08	0.11	31.31
J160100.43+044236.3	4808-55705-0318	0.77	14744	11500	44.79	28.35	-0.28	7.60
J155708.02+041156.4	4808-55705-0466	1.19	22483	23000	40.70	9.41	-0.08	60.16
J110341.38+053448.9	4855-55926-0376	1.07	11687	10500	16.41	2.81	-0.33	72.64
J090139.03+064022.4	4868-55895-0730	0.88	6621	8000	0.80	0.00	-0.20	17.50

Table 2 continued on next page

Table 2 (continued)

SDSS	Plate-MJD-Fiber	M	T _{eff}	T _{SDSS}	B	$\sigma(B)$	z _{offset}	incl
		(M _⊙)	(K)	(K)	(MG)	(MG)	(R _*)	(°)
J151415.65+074446.4	4878-55710-0747	—	—	10000	37.07	11.91	-0.32	49.14
J154626.16+143754.8	4890-55741-0988	0.62	36702	30000	2.99	0.40	0.42	88.92
J155835.80+122139.4	4901-55711-0358	0.58	25321	24000	2.13	0.58	-0.30	88.31
J153049.68+344434.7	4975-56037-0762	1.13	25710	37472	10.43	5.91	-0.47	63.27
J153948.03+404528.5	4976-56046-0553	0.74	16617	12500	18.84	2.75	-0.35	59.56
J170751.91+353239.4	4988-55825-0107	1.13	21596	18000	2.64	0.43	-0.38	53.27
J171102.58+360959.6	4989-55743-0414	0.66	23378	20546	2.30	0.07	0.11	14.34
J170123.81+330853.9	4992-55723-0866	—	—	12206	37.71	1.24	-0.32	0.92
J171959.47+331614.9	4994-55739-0097	0.63	28249	21000	2.20	0.22	0.22	88.33
J172432.14+323414.9	5002-55710-0601	1.22	24779	22000	257.20	43.61	-0.20	50.29
J163036.79+272451.5	5005-55751-0254	1.03	10762	11500	35.60	6.30	-0.19	52.96
J171711.53+262012.0	5016-55709-0596	1.14	20593	22000	18.49	0.57	-0.36	52.32
J224741.46+145638.7	5040-56243-0482	1.09	16732	18000	515.09	72.32	0.21	28.92
J221141.80+113604.5	5064-55864-0122	1.34	9574	9500	18.77	1.05	-0.35	22.29
J010405.12+145907.3	5131-55835-0438	0.48	13897	10500	2.78	0.20	0.31	89.97
J010311.32+151110.0	5131-55835-0578	0.35	12457	11000	2.81	0.16	-0.42	67.41
J012646.78+193454.5	5135-55862-0886	0.97	8393	8000	2.22	0.13	-0.09	52.27
J011423.35+160727.6	5139-55866-0410	—	—	22000	22.97	13.33	0.06	46.94
J150813.26+394505.1	5167-56066-0732	—	—	29032	12.95	9.75	-0.05	15.13
J144405.60+405338.0	5172-56071-0676	0.57	23688	25000	2.56	0.12	-0.17	75.76
J145330.84+390245.2	5174-56047-0828	0.52	15751	13500	2.29	0.13	0.31	77.93
J084330.81+201049.1	5176-56221-0564	0.73	47864	25000	21.52	2.13	-0.42	0.02
J085649.67+253441.0	5179-55957-0778	0.92	10783	11500	85.00	11.68	-0.20	19.31
J164342.37+315728.7	5194-56062-0546	0.51	20438	15500	2.25	0.08	0.29	73.53
J164703.23+370910.2	5198-55823-0511	0.84	15954	16500	3.01	0.17	-0.42	47.55
J161710.49+383306.9	5199-56067-0720	0.58	12988	16500	2.45	0.10	0.29	76.34
J160531.60+385210.0	5200-56091-0678	0.48	15025	13000	2.67	0.11	0.38	13.62
J154238.25+101156.9	5206-56033-0032	0.45	14715	11500	2.56	0.08	-0.37	72.58
J083656.62+103452.1	5284-55866-0690	0.53	17638	17000	2.07	0.14	0.10	47.85
J085820.01+103725.4	5291-55947-0999	0.61	17808	20000	2.14	0.55	0.09	17.15
J085523.86+164058.9	5292-55926-0186	0.74	12741	12000	11.04	0.58	-0.44	20.88
J085841.78+074728.3	5294-55922-0180	—	—	18000	2.52	0.00	0.25	0.00
J090827.08+092100.2	5299-55927-0834	1.14	26638	40000	46.50	28.29	0.14	64.68
J091239.63+102645.7	5302-55896-0230	0.40	19030	16000	3.10	0.06	0.44	11.60
J092417.96+142238.2	5305-55984-0002	0.69	19279	30000	2.38	0.13	0.11	4.05
J093707.06+102149.1	5316-55955-0434	1.21	19695	17500	394.67	127.88	0.43	42.94
J094004.19+123930.8	5318-55983-0468	—	—	8000	2.19	0.03	-0.28	63.18
J103336.57+105710.9	5346-55955-0628	0.46	6526	8000	24.10	9.90	-0.31	2.62
J105055.04+143359.4	5355-56009-0532	0.28	16510	15500	2.81	0.20	0.40	23.74
J112605.90+090628.8	5371-55976-0258	1.05	10197	10500	32.12	42.07	-0.19	9.25

Table 2 continued on next page

Table 2 (continued)

SDSS	Plate-MJD-Fiber	M	T _{eff}	T _{SDSS}	B	$\sigma(B)$	Z _{offset}	incl
		(M _⊙)	(K)	(K)	(MG)	(MG)	(R _*)	(°)
J112148.80+103934.2	5371-55976-0512	0.98	11385	17000	311.79	61.86	-0.12	86.65
J120125.38+084800.3	5389-55953-0671	0.80	7395	8000	2.15	0.08	-0.10	11.69
J121735.25+082810.0	5393-55946-0981	1.06	18534	15000	2.57	0.39	-0.38	58.03
J123531.30+154418.2	5404-56013-0896	0.94	7443	8000	50.74	16.26	-0.15	26.27
J124058.11+063645.6	5407-55926-0250	0.58	15283	11000	2.08	0.17	0.10	32.16
J124852.85+153641.9	5414-56014-0423	0.75	22844	14000	2.70	0.17	0.25	3.76
J131508.96+093713.8	5426-55987-0342	0.86	20370	22000	12.93	8.36	-0.50	18.22
J131802.48+071743.2	5429-55979-0448	0.41	21840	15500	3.17	0.05	0.46	4.43
J133156.48+124055.9	5432-56008-0858	0.55	18585	20000	2.28	0.29	-0.18	76.37
J133738.54+072440.2	5437-55973-0404	0.44	15184	13500	3.15	0.20	0.46	3.59
J135107.02+074345.5	5442-55978-0132	1.15	14421	9500	2.19	0.04	-0.23	58.02
J135048.10+084512.6	5442-55978-0820	0.58	6715	8000	2.15	0.08	-0.10	47.65
J134845.98+110008.8	5445-55987-0530	1.21	18493	16500	202.58	14.94	0.19	4.31
J135204.28+112055.2	5445-55987-0622	0.61	16139	18000	2.35	0.07	0.16	89.99
J141307.56+121537.4	5453-56001-0030	0.71	40664	30000	2.96	0.29	-0.44	74.88
J142003.63+103930.4	5456-55980-0016	0.60	14854	12500	2.26	0.11	0.32	86.15
J142035.36+112042.2	5460-56000-0598	0.87	19953	13000	3.00	0.11	0.43	15.18
J142708.16+100910.9	5465-55988-0464	0.45	15291	16500	2.23	0.17	0.26	65.73
J143506.35+072940.3	5467-55973-0321	0.34	11759	11500	2.54	0.08	-0.37	73.66
J150957.07+092349.3	5487-55982-0596	1.07	10003	10000	6.00	0.25	-0.17	9.06
J085419.97+603701.6	5709-56571-0108	0.93	10293	11000	62.99	10.03	-0.19	12.15
J091015.08+520310.7	5732-56326-0864	0.56	18471	19500	2.41	0.12	-0.28	29.69
J085817.39+471501.2	5735-55980-0410	0.53	19803	10317	2.82	0.14	-0.42	63.34
J090205.29+454915.5	5736-55984-0466	0.63	10928	11000	2.83	0.30	-0.44	56.63
J094235.02+205208.2	5786-56251-0182	1.15	23252	15500	62.79	26.23	-0.18	62.95
J134913.52+205646.9	5869-56064-0446	0.93	9462	11413	385.05	34.49	-0.08	69.00
J104219.06+203008.7	5874-56039-0134	1.12	24656	40000	128.98	100.74	0.03	46.61
J105544.90+211105.0	5876-56042-0550	—	—	8000	0.50	0.00	-0.25	6.98
J113409.06+182238.7	5879-56047-0108	—	—	8500	2.24	0.03	-0.5	1.27
J114441.65+171716.4	5892-56035-0686	0.78	17884	23000	2.15	0.21	-0.20	11.84
J073341.55+435348.0	5942-56210-0336	—	—	11500	46.57	7.90	-0.15	65.31
J215425.28+272109.5	5964-56098-0187	0.66	6353	8000	17.94	6.33	-0.47	12.61
J124751.79+262110.2	5987-56339-0712	0.76	7197	8000	43.21	27.89	-0.13	21.35
J141604.48+235404.2	6013-56074-0656	0.63	15687	14000	2.27	0.36	0.30	76.82
J143122.55+261026.4	6017-56075-0646	—	—	9500	2.03	0.03	0.10	27.59
J145829.87+223040.6	6020-56087-0312	0.91	9255	9500	32.53	10.51	-0.15	62.98
J144331.21+262423.9	6022-56076-0670	0.66	15764	40000	4.78	0.20	0.50	3.19
J164843.29+461803.7	6027-56103-0970	0.76	13011	12500	18.04	1.23	-0.34	41.90
J163900.06+440808.0	6030-56097-0034	0.47	14074	13000	2.85	0.17	0.39	15.02
J163458.64+415820.0	6036-56093-0308	0.61	18154	24000	2.06	0.23	-0.13	52.66

Table 2 continued on next page

Table 2 (*continued*)

SDSS	Plate-MJD-Fiber	M	T _{eff}	T _{SDSS}	B	$\sigma(B)$	Z _{offset}	incl
		(M _⊙)	(K)	(K)	(MG)	(MG)	(R _*)	(°)
J151130.16+422022.9	6048-56072-0374	1.02	10945	11500	12.83	16.96	-0.28	34.91
J224912.31+220910.4	6120-56206-0747	0.46	12735	17500	2.14	0.07	-0.28	84.78
J233958.11+154419.8	6138-56236-0466	—	—	10000	3.15	0.00	-0.05	49.87
J232136.69+133133.5	6142-56219-0001	0.65	14033	10500	2.57	0.13	-0.38	56.25
J231940.37+140121.1	6142-56219-0110	—	—	17500	3.00	0.07	0.43	18.05
J233052.97+143037.5	6143-56267-0900	—	—	23000	17.50	1.62	-0.46	9.02
J230119.48+101939.0	6154-56237-0386	—	—	9000	7.34	0.04	-0.08	36.48
J233817.93+083732.6	6161-56238-0622	0.72	11534	10500	118.33	62.08	-0.38	7.12
J000505.48+183548.0	6170-56240-0212	—	—	11500	2.15	0.01	-0.10	67.88
J001112.41+155209.5	6178-56213-0312	0.54	19975	15000	3.38	0.02	0.50	2.61
J004104.51+303819.4	6252-56248-0866	—	—	9000	2.00	0.02	0.14	2.24
J225828.48+280828.8	6293-56561-0264	1.02	10618	10500	137.09	33.81	-0.35	44.67
J222348.44+231909.3	6299-56478-0639	0.90	8589	8500	6.00	1.11	-0.50	14.66
J113136.70+242122.8	6421-56274-0804	0.80	9863	11500	78.38	15.07	-0.13	60.34
J103036.02+225011.4	6425-56298-0386	1.11	17019	10000	5.33	0.02	-0.50	20.23
J114246.50+205221.9	6432-56309-0563	0.97	12631	10000	74.76	10.78	-0.11	57.33
J101712.60+233646.6	6458-56274-0968	1.04	10843	11500	143.03	15.18	-0.34	60.06
J140750.65+301130.2	6495-56339-0886	1.18	21841	23000	86.00	10.48	-0.07	27.98
J234858.29+253519.0	6518-56567-0796	0.92	23407	15500	7.68	0.78	-0.50	33.38
J124906.90+432543.0	6617-56365-0033	1.05	63789	30000	2.76	0.25	-0.41	69.68
J125232.05+423210.8	6619-56371-0368	—	—	30000	2.57	0.24	-0.37	63.32
J134131.64+440030.0	6626-56330-0744	0.76	7240	8000	40.62	80.27	-0.21	6.54
J124322.38+450002.0	6635-56370-0334	0.87	12305	9500	48.22	36.92	-0.12	49.92
J114828.99+482731.1	6678-56401-0952	1.26	33083	30000	41.58	134.21	0.37	27.36
J125121.86+543215.7	6679-56401-0398	0.57	8563	8500	13.85	0.40	-0.46	41.29
J115244.11+501844.5	6683-56416-0330	0.91	9499	9500	14.65	0.42	-0.43	62.27
J134758.88+495427.4	6744-56399-0957	0.82	15798	16628	2.29	0.23	-0.30	72.13
J140716.66+495613.7	6746-56386-0678	1.03	19650	18500	15.43	0.48	0.41	89.92
J133819.06+624018.7	6816-56444-0668	0.65	11191	13000	40.00	4.22	-0.25	8.42
J134043.10+654349.2	6825-56717-0206	0.67	13462	11500	3.27	0.22	-0.50	31.50
J132208.55+551939.0	6828-56430-0780	0.98	12240	9500	2.91	1.34	-0.22	44.31
J000825.77-054122.3	7035-56568-0241	—	—	30000	2.58	0.08	-0.35	77.82
J025001.76-043703.1	7054-56575-0438	1.16	12603	19000	309.41	38.57	0.15	42.50
J025506.13-071551.4	7059-56592-0652	0.72	7322	8000	9.00	1.41	-0.28	6.99
J103655.38+652252.0	7083-56722-0200	1.21	21677	19500	15.37	1.27	-0.49	3.71
J101400.72+594933.1	7087-56637-0772	0.43	6906	8000	1.90	0.04	-0.23	6.85
J102553.68+622929.1	7090-56659-0696	0.91	8255	9000	3.25	0.01	-0.48	46.08
J114152.02+572000.9	7092-56683-0812	—	—	11000	2.49	0.01	-0.23	52.09
J111528.74+570125.3	7100-56636-0430	0.97	23414	23000	2.19	0.34	-0.25	72.44
J120150.14+614256.8	7106-56663-0100	0.87	9702	10500	14.72	1.54	-0.49	53.43

Table 2 *continued on next page*

Table 2 (continued)

SDSS	Plate-MJD-Fiber	M	T _{eff}	T _{SDSS}	B	$\sigma(B)$	z _{offset}	incl
		(M _⊙)	(K)	(K)	(MG)	(MG)	(R _*)	(°)
J115917.38+613914.2	7106-56663-0132	1.20	21001	17000	16.73	0.23	-0.37	49.20
J132858.19+590851.0	7117-56685-0012	1.20	24259	18000	15.43	1.34	-0.50	1.59
J122739.16+661224.3	7120-56720-0426	0.76	20248	19000	24.27	4.90	-0.40	49.18
J123159.51+670918.9	7120-56720-0653	0.23	20220	14500	3.45	0.56	0.49	3.91
J224459.60+331017.3	7142-56567-0966	1.22	20263	20000	421.87	13.77	0.30	44.69
J000555.90-100213.5	7167-56604-0030	1.20	26711	25000	8.30	0.90	-0.50	40.47
J021205.31+064420.5	7256-56658-0740	1.15	13881	19000	34.00	22.68	-0.44	8.65
J093832.79+474050.6	7307-56720-0130	0.96	10251	12500	90.34	54.26	-0.43	16.43
J100657.97+484506.0	7329-56719-0825	—	—	9000	23.97	0.18	0.24	4.72
J094026.71+631427.6	7447-56746-0198	0.81	14126	11000	2.81	0.18	-0.36	72.90
J215209.66+223039.3	7576-56948-0399	0.87	8189	8500	7.25	0.18	-0.39	45.28

REFERENCES

- Astropy Collaboration, Robitaille, T. P., Tollerud, E. J., et al. 2013, *A&A*, 558, A33, doi: [10.1051/0004-6361/201322068](https://doi.org/10.1051/0004-6361/201322068)
- Astropy Collaboration, Price-Whelan, A. M., Sipőcz, B. M., et al. 2018, *AJ*, 156, 123, doi: [10.3847/1538-3881/aabc4f](https://doi.org/10.3847/1538-3881/aabc4f)
- Babcock, H. W. 1947, *ApJ*, 105, 105, doi: [10.1086/144887](https://doi.org/10.1086/144887)
- . 1958, *ApJS*, 3, 141, doi: [10.1086/190035](https://doi.org/10.1086/190035)
- Bagnulo, S., & Landstreet, J. D. 2021, *MNRAS*, 507, 5902, doi: [10.1093/mnras/stab2046](https://doi.org/10.1093/mnras/stab2046)
- . 2022, *ApJL*, 935, L12, doi: [10.3847/2041-8213/ac84d3](https://doi.org/10.3847/2041-8213/ac84d3)
- Belloni, D., & Schreiber, M. R. 2020, *MNRAS*, 492, 1523, doi: [10.1093/mnras/stz3601](https://doi.org/10.1093/mnras/stz3601)
- Gentile Fusillo, N. P., Tremblay, P. E., Cukanovaite, E., et al. 2021, *MNRAS*, 508, 3877, doi: [10.1093/mnras/stab2672](https://doi.org/10.1093/mnras/stab2672)
- Ginzburg, S., Fuller, J., & Kawka, A. 2022, arXiv e-prints, arXiv:2202.12902. <https://arxiv.org/abs/2202.12902>
- Greenstein, J. L., Gunn, J. E., & Kristian, J. 1971, *ApJL*, 169, L63, doi: [10.1086/180814](https://doi.org/10.1086/180814)
- Horowitz, C. J., Schneider, A. S., & Berry, D. K. 2010, *PhRvL*, 104, 231101, doi: [10.1103/PhysRevLett.104.231101](https://doi.org/10.1103/PhysRevLett.104.231101)
- Isern, J., García-Berro, E., Külebi, B., & Lorén-Aguilar, P. 2017, *ApJL*, 836, L28, doi: [10.3847/2041-8213/aa5eae](https://doi.org/10.3847/2041-8213/aa5eae)
- Kawka, A. 2020, *IAU Symposium*, 357, 60, doi: [10.1017/S1743921320000745](https://doi.org/10.1017/S1743921320000745)
- Kemp, J. C., Swedlund, J. B., Landstreet, J. D., & Angel, J. R. P. 1970, *ApJL*, 161, L77, doi: [10.1086/180574](https://doi.org/10.1086/180574)
- Kepler, S. O., Koester, D., Pelisoli, I., Romero, A. D., & Ourique, G. 2021, *MNRAS*, 507, 4646, doi: [10.1093/mnras/stab2411](https://doi.org/10.1093/mnras/stab2411)
- Kepler, S. O., Pelisoli, I., Jordan, S., et al. 2013, *MNRAS*, 429, 2934, doi: [10.1093/mnras/sts522](https://doi.org/10.1093/mnras/sts522)
- Kilic, M., Kosakowski, A., Moss, A. G., Bergeron, P., & Conly, A. A. 2021, arXiv e-prints, arXiv:2111.14902. <https://arxiv.org/abs/2111.14902>
- Külebi, B., Jordan, S., Euchner, F., Gänsicke, B. T., & Hirsch, H. 2009, *A&A*, 506, 1341, doi: [10.1051/0004-6361/200912570](https://doi.org/10.1051/0004-6361/200912570)
- Lauffer, G. R., Romero, A. D., & Kepler, S. O. 2018, *MNRAS*, 480, 1547, doi: [10.1093/mnras/sty1925](https://doi.org/10.1093/mnras/sty1925)
- Liebert, J. 1988, *PASP*, 100, 1302, doi: [10.1086/132322](https://doi.org/10.1086/132322)
- Liebert, J., Bergeron, P., & Holberg, J. B. 2003, *AJ*, 125, 348, doi: [10.1086/345573](https://doi.org/10.1086/345573)
- Liebert, J., & Sion, E. M. 1979, *Astrophys. Lett.*, 20, 53
- McCleery, J., Tremblay, P.-E., Gentile Fusillo, N. P., et al. 2020, *MNRAS*, 499, 1890, doi: [10.1093/mnras/staa2030](https://doi.org/10.1093/mnras/staa2030)
- Romero, A. D., Kepler, S. O., Córscico, A. H., Althaus, L. G., & Fraga, L. 2013, *ApJ*, 779, 58, doi: [10.1088/0004-637X/779/1/58](https://doi.org/10.1088/0004-637X/779/1/58)
- Schimeczek, C., & Wunner, G. 2014, *ApJS*, 212, 26, doi: [10.1088/0067-0049/212/2/26](https://doi.org/10.1088/0067-0049/212/2/26)
- Schreiber, M. R., Belloni, D., Gänsicke, B. T., & Parsons, S. G. 2021, *MNRAS*, 506, L29, doi: [10.1093/mnras/lsab069](https://doi.org/10.1093/mnras/lsab069)

Tout, C. A., Wickramasinghe, D. T., Liebert, J., Ferrario,

L., & Pringle, J. E. 2008, MNRAS, 387, 897,

doi: [10.1111/j.1365-2966.2008.13291.x](https://doi.org/10.1111/j.1365-2966.2008.13291.x)

Valyavin, G., & Fabrika, S. 1999, in Astronomical Society of the Pacific Conference Series, Vol. 169, 11th European Workshop on White Dwarfs, ed. S. E. Solheim & E. G. Meistas, 206

Wickramasinghe, D. T., & Ferrario, L. 2005, MNRAS, 356, 1576, doi: [10.1111/j.1365-2966.2004.08603.x](https://doi.org/10.1111/j.1365-2966.2004.08603.x)

Williams, K. A., Hermes, J. J., & Vanderbosch, Z. P. 2022, arXiv e-prints, arXiv:2207.13763.

<https://arxiv.org/abs/2207.13763>